

Article

New, Amino Acid Based Zwitterionic Polymers as Promising Corrosion Inhibitors of Mild Steel in 1 M HCl

Mohammad A. Jafar Mazumder 

Chemistry Department, King Fahd University of Petroleum and Minerals, Dhahran 31261, Saudi Arabia; jafar@kfupm.edu.sa; Tel.: +966-13-860-7836; Fax: +966-13-860-4277

Received: 22 September 2019; Accepted: 11 October 2019; Published: 17 October 2019



Abstract: The zwitterionic monomers, *N,N'*-diallylamino propanephosphonate and amino acid residual *N,N'*-diallyl-L-methionine hydrochloride were synthesized, with excellent yields. These monomers were utilized in the preparation of zwitterionic homo and co-cyclopolymers 5–7 in aqueous solution using 2,2'-azobis (2-methylpropionamide) dihydrochloride as an initiator. The polymers were characterized by FT-IR, NMR, and TGA. The performance of these synthesized polymers on mild steel in acidic solution was investigated by gravimetric method, Tafel extrapolation, linear polarization resistance, and electrochemical impedance spectroscopy. At 313 K, the maximum inhibition efficiencies of corrosion inhibitors 5–7 at 4.50×10^{-4} mol L⁻¹ were found to be 85.2%, 83.3%, and 99.5%, respectively. The inhibition efficiencies obtained from gravimetric weight loss, potentiodynamic polarization, and electrochemical impedance spectroscopy measurements were in good agreement. Different adsorption isotherms were also explored to find the best fit, and found to obey Langmuir adsorption isotherm. The thermodynamic parameters, such as activation energy (E_a), standard enthalpy of activation (ΔH^*), standard entropy of activation (ΔS^*), adsorption–desorption equilibrium constant (K_{ads}), and standard free energy of adsorption (ΔG°_{ads}), were determined. Electrochemical data indicated that the zwitterionic copolymer 7 acts as a mixed type inhibitor under the influence of anodic control. The surface morphology of mild steel corrosion was evaluated without and with corrosion inhibitors by AFM, SEM-EDX, and XPS, which confirmed the adsorption of inhibitor molecules on the metal surface.

Keywords: cyclopolymerization; water-soluble polymers; zwitterionic polymers; corrosion inhibitors; potentiodynamic polarization; adsorption isotherm; acidic medium; mild steel

1. Introduction

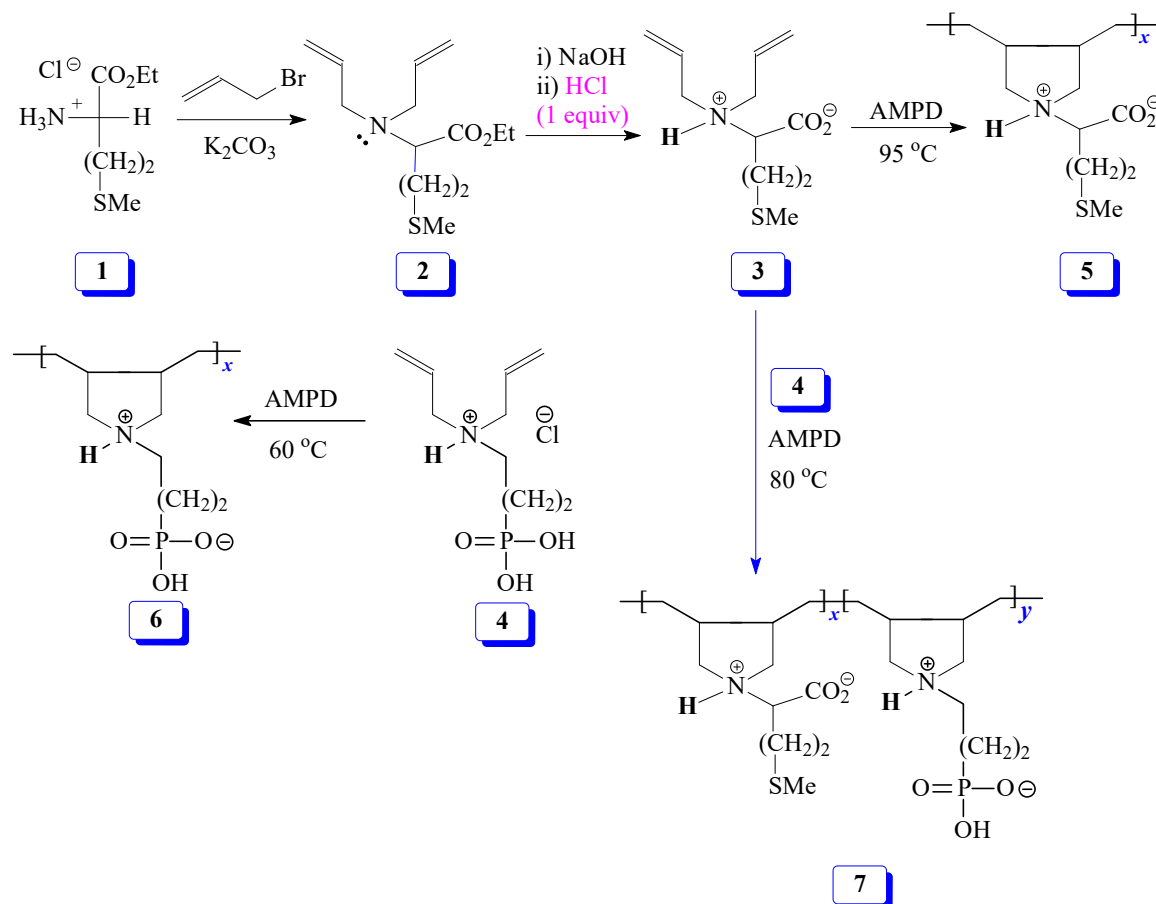
The inexpensive and readily available mild steel has very high iron content (>99%), which has been appeared as a subject of durative studies in the field of corrosion due to its high mechanical and technological values, and found huge industrial applications, particularly in petroleum industries [1]. Corrosion is considered a destructive process of metal and alloys, which occurs due to chemical and electrochemical reactions with the companion environments. It is an aggressive process, and generates constant, continuous and huge financial costs to health and the environment, and safety losses for the industrial and metallic resources that eventually appear with a great concern to both industry and society [2]. In most cases, it is very difficult to eliminate completely. A recent worldwide study conducted by National Association of corrosion Engineers (NACE) estimated that the yearly cost of corrosion is approximately 2.5 trillion US dollars, which is approximately 4.2% of the total gross domestic product [3]. Considering the impacts on health and safety, and economic losses, different kinds of preventative technologies have been developed and implemented, depending upon the nature of metal, to control, reduce, or eliminate corrosion.

Mild steel is very vulnerable towards corrosion with continuous exposure to acids, particularly hydrochloric acid (HCl) in different industrial processes [4]. In most cases, HCl has been used to remove rusts, scales, and sludges. Additionally, HCl is used in oil-well in oil and gas industries, industrial cleaning purposes, acid pickling, and impregnating different metallic compounds [5,6]. These days, the use of synthetic corrosion inhibitors is one of the most reliable, convenient, and handy methods for the protection of mild steel from corrosion in acidic environments, due to convenient and effective synthesis procedures and use; easy-to-achieve, tunable properties; and economical value [7,8]. Varieties of corrosion inhibitors (organic and inorganic) are widely explored to realize their inhibitive effects on metallic corrosion in different corrosive environments [9].

The heteroatom-containing organic corrosion inhibitors are used to protect mild steel from corrosion. The efficacy order of these heteroatoms is identified as $P > S > N > O$ [10]. However, the application of these small molecule corrosion inhibitors is limited due to the fact that they are toxic and not environmentally friendly [11]. In recent years, polymers containing the heteroatoms N, O, S, or P have received particular attention as corrosion inhibitors due to their availability, cost effectiveness, stability, and the availability of multiple attaching sites in the polymer backbone and/or in the pendants. The multifunctional anchoring sites of atoms and/or functional groups present in the polymer chain can easily attach/adsorb on the metal surface [12], thereby protecting the metal surface from the corrosive environment [13]. Moreover, polymers are usually less toxic and adsorb more strongly than their monomer analogs [14,15]. It is expected that polymers can act as better inhibitors for protecting metal corrosion than their corresponding low molecular organics/monomers [16]. Biocompatible amino acids have been used in pharmaceuticals and biological applications for many decades [17]. The amino acids, particularly methionine, have been reported as effective green corrosion inhibitors in different aggressive media [18–20]. Methionine has been studied for mild steel corrosion, and its inhibition efficiency at concentrations of 25, 149, and 746 ppm was reported to be 47% in 0.1 M HCl at 25 °C [21], 89% in 1 M HCl at 30 °C [22], and 54.8% in 0.5 M H₂SO₄ at 30 °C [23], respectively. Methionine methyl ester hydrochloride was studied in 1 M HCl at 30 °C for mild steel corrosion, and the inhibition efficiency at a concentration of 923 ppm was found to be 81.2% [24]. Methionine, methionine sulfoxide, and methionine sulfone at a respective concentrations of 149, 165, and 181 ppm in 1 M HNO₃ at 30 °C have been shown to attain an inhibition efficiency of 79, 85, and 88%, respectively [25]. A literature surveys showed that there are numerous research articles that dealt with N, O, S, or P-containing compounds for metallic corrosion inhibition [26–28], but so far, no report is available that deals with all four heteroatoms (N, O, S, and P) in a single polymer, based on residual methionine, for effective metallic corrosion inhibition.

This article aims to study the influence of S, N, and O in amino acid methionine and P, N, and O in phosphonic acid on the corrosion inhibition performance of mild steel in acid solution. The more polarizable third period elements (S and P) can utilize their lone pairs of electrons to form coordinate type bonds with the vacant *d*-orbitals of Fe or Fe²⁺ on the metal surface [29], thereby interfering anodic or cathodic reactions responsible for corrosion [30]. We anticipate that the inclusion of five membered pyrrolidine motifs having methionine residues and phosphonic acid groups in a polymeric chain might enhance the ability to provide better surface coverage and protection from corrosive media. The pyrrolidine motifs of a five-membered ring attached to the polymer backbone is considered one of the major synthetic polymer architectures used in many applications [31]. Here, we report the synthesis of homo and co-cyclopolymers of *N,N'*-diallylamino propanephosphonic acid and the amino acid residues of hydrolyzed methionine (Scheme 1) using Butler's cyclopolymerization protocol [32–34]. We studied the inhibitive actions of these new synthetic polymers to suppress the corrosion of mild steel in 1 M hydrochloric acid solution. In addition to O, S, and P, the quaternized N and other attaching points present in the macromolecular chain gave us an opportunity to evaluate their inhibition efficiencies as a potential corrosion inhibitor in aqueous acidic solution. The inhibition efficiencies and adsorption behavior of these newly synthesized zwitterionic polymers on mild steel corrosion were studied by gravimetric, potentiodynamic polarization and electrochemical impedance spectroscopy (EIS) methods,

and the surface morphology was evaluated by atomic force microscopy (AFM) (Nanosurf, Woburn, MA, USA), x-ray photoelectron spectroscopy (XPS) (250 Xi, Kansas, MN, USA), and scanning electron microscopy (SEM) (FESEM, Lyra 3, Tescan, Czech Republic) and energy dispersive x-ray spectroscopy (EDX) (Oxford Inc., UK).



Scheme 1. The synthesis of monomers and polymers.

2. Materials and Methods

2.1. Materials

The ethyl ester hydrochloride of L-methionine (**1**) was obtained from Fluka Chemie AG (Buchs, Switzerland). Hydrochloric acid (HCl, 37% *w/v*), sodium hydroxide (NaOH), acetic acid, sodium chloride, sodium sulfate, and potassium carbonate (K_2CO_3) were purchased from BDH Chemical Ltd. (Poole, UK) and used as received. Allyl bromide, ammonium persulfate (APS), and 2,2'-azobis(2-methylpropionamide) dihydrochloride (AMPD) (Fluka Chemie AG) were used as received. Triethyl phosphate, 1,3-dibromopropane, and diallylamine were purchased from Sigma Aldrich (St. Louis, MO, USA), and used as received. Dimethyl sulfoxide (DMSO) was dried and distilled (bp_{4 mmHg} 64–65 °C). Acetonitrile, diethyl ether, acetone, toluene, methanol, and ethanol from Fluka AG and were used as received. All solvents were of HPLC grade. Diallyl derivative of methionine monomer **2** [35] and its zwitterionic species **3** [36] were prepared from L-methionine ethyl ester hydrochloride **1** as described. 3-(*N,N'*-Diallylammonio) propane phosphonate **4** [37] and its polyzwitterionic acid (PZA) **6** [38] were synthesized according to previously published procedure. Their sequence is presented in Scheme 1. Distilled de-ionized water was used to prepare a 1 M HCl solution from concentrated HCl (37%). The freshly prepared 1 M HCl solution was used to prepare

different concentrations of corrosion inhibitor solutions. Note that the 1 M HCl solution in the absence of corrosion inhibitor was used as blank.

2.2. Physical Methods

Perkin Elmer 16F PC Fourier transform infrared spectroscopy (FT-IR) (Waltham, MA, USA) was used to record IR spectra, while ^1H and ^{13}C NMR were collected in a JEOL 500 MHz Nuclear Magnetic Resonance (NMR) spectrometer (Peabody, MA, USA). The elemental composition of the synthesized compounds was determined by Perkin Elmer elemental analyzer (Carlo-Erba, model 2400, Waltham, MA, USA). An Ubbelohde viscometer having viscometer constant $0.005317 \text{ mm}^2 \text{ s}^{-2}$ was used to determine the intrinsic viscosity in 0.1 M NaCl at 30°C . The TA instruments SDT thermogravimetric analyzer (model Q600, Newcastle, USA) with step up temperature: $10^\circ\text{C}/\text{min}$, range: $20\text{--}800^\circ\text{C}$, and platinum/platinum–rhodium (Type R) thermocouples under N_2 (flow rate 50 mL min^{-1}), was used for thermogravimetric analysis (TGA). All electrochemical measurements were captured by Auto Lab potentiostat-galvanostat (model 10A-BST707A, Eco Chemie, Netherlands). Surface tension was measured using a surface tensiometer (PHYWE, Göttingen, Germany) equipped with a torsion dynamometer (0.01 N) and platinum iridium ring having a diameter of 1.88 cm.

2.3. Synthesis

2.3.1. Synthesis of Hydrolyzed Methionine Homopolymer (5)

The amino acid residue of methionine sulfide containing zwitterionic polymer was prepared following the Butler's cyclopolymerization protocol [32,35]. The zwitterionic monomer **3** (2.13 g, 9.29 mmol), and AMPD (0.299 g, 1.10 mmol) were dissolved in 0.135 g de-ionized water and 1.04 g concentrated HCl (37%) in a 10-mL round bottom flask. The pure N_2 gas was bubbled into the reaction mixture for 5 min, then stirred the reaction mixture at 95°C for 2 h. After completion of the reaction, the crude polymer was dissolved in de-ionized water (4 mL) and dialyzed against 0.1 M HCl for 18 h; the purified polymer **5** was then freeze-dried. Yield: 1.92 g (90%). The thermal decomposition of zwitterionic homopolymers **5**: $240\text{--}250^\circ\text{C}$ (decomposed, turned brown). FT-IR: ν_{max} . (KBr) 3437, 3018, 2926, 2857, 1624, 1455, 1393, 1278, 1129, 1067, 1020, 877, 779, 656, and 563 cm^{-1} . ^1H NMR: δ_{H} (D_2O) 1.09 (4H, m), 1.28 (2H, m), 1.99 (3H, s), 2.12 (2H, m), 2.54 (2H, m), 3.35–3.99 (5H, m). ^{13}C NMR: δ_{C} (D_2O) 15.1 (1C, SCH_3), 26.5 (1C, $\text{CH}_2\text{CH}_2\text{S}$), 30.8 (1C, $\text{CH}_2\text{CH}_2\text{S}$), 40.3 (2C, CHCH_2), 55.8 (2C, CHCH_2), 59.4 (2C, NCH_2), 70.4 (1C, NCH), and 173.1 (1C, CO_2) (67.4, dioxane).

2.3.2. Synthesis of Zwitterionic Copolymers of 3-(N,N' diallylamino) Propanephosphonic Acid and N,N' -diallyl-1-methionine Ethanoate (7)

A mixture of amino acid residues of hydrolyzed methionine **3** (2.29 g, 10.0 mmol) and 3-(N,N' -diallylamino)-propanephosphonic acid (2.55 g, 10.0 mmol) was dissolved in 1.57 g H_2O and 1.09 g HCl (37%, 11.0 mmol) in 25 mL round bottom flask. AMPD (0.269 g, 0.992 mmol) was then added to the reaction mixture. The solution was gently bubbled with N_2 for 5 min. Then, we heated the flask at 80°C for 40 h. After completion of the reaction, the resultant crude polymer was dialyzed against deionized water for 15 h, and then freeze-dried. The isolated zwitterionic copolymer **7** was obtained as a white powder. Yield: 3.29 g (68%). The thermal decomposition of zwitterionic copolymer **7**: $250\text{--}270^\circ\text{C}$ (decomposed, turned black). FT-IR: ν_{max} . (KBr) 3431, 2930, 2854, 2589, 1627, 1458, 1390, 1301, 1141, 1048, 899, 772, 654, and 536 cm^{-1} . ^1H NMR: δ_{H} (D_2O) 0.89 (2H, m), 1.07 (4H, m), 1.23 (2H, t), 1.52 (4H, m), 1.79 (3H, s), 2.11 (2H, m), 2.46 (2H, m), 2.83–3.40 (5H, m). ^{13}C NMR: δ_{C} (D_2O) 15.1 (1C), 20.6 (1C), 25.2 (1C), 26.2 (1C), 29.7 (1C), 34.5 (1C), 37.4 (1C), 40.8 (2C), 44.0 (2C), 58.4 (2C), 55.8 (2C), 70.2 (2C), 70.9 (2C), and 173.3 (1C) (67.4, dioxane).

2.4. Mild Steel Coupon

Corrosion inhibition experiments were conducted on mild steel coupons. The percentage of chemical compositions is depicted in Table 1. For gravimetric weight loss studies, rectangularly shaped mild steel coupons were cut from large steel sheet into the dimensions 2.5 cm × 2.0 cm × 0.1 cm, and abraded with SiC emery papers of grit sizes 100, 600, and 1500, then washed with deionized water, degreased in acetone and dried in a vacuum oven at 60 °C, and finally, stored in an airtight oven before use. For potentiodynamic polarization and electrochemical impedance studies, flag shaped mild steel coupons were mechanically cut to dimensions 1.0 cm × 1.0 cm × 0.1 mm, abraded, and cleaned following the similar procedure described above (for weight loss study), having approximately 3 cm long stem embedded by Araldite resin.

Table 1. The chemical composition of mild steel coupon.

Elements	C	Mn	Cr	Ni	Mo	Cu	V	P	Fe
wt.%	0.089	0.34	0.037	0.022	0.007	0.005	0.005	0.010	99.47

2.5. Corrosion Tests

2.5.1. Gravimetric Weight Loss Experiments

The gravimetric weight loss experiments were carried out at different temperatures (313–333 K) using rectangular shaped mild steel coupons of almost equal sizes (2.5 cm × 2.0 cm × 0.1 cm). A different temperature was chosen to represent the ranges usually used in 1 M HCl to afford comparable data between the corrosion inhibitors. The accurately weighed mild steel samples were dipped in 1 M HCl (250 mL) without or with different concentrations (3.75×10^{-6} – 4.50×10^{-4} mol L⁻¹) of corrosion inhibitors 5–7 without stirring. After 6 h of immersion, the mild steel coupons were removed from 1 M HCl, thoroughly washed with deionized water and acetone, dried, and weighed. The average values of weight loss were calculated from three mild steel samples obtained from three individual experiments at each concentration. The standard deviations of the average weight loss data varied within a range of 0.7–3.0%.

2.5.2. Electrochemical Experiments

The electrochemical experiments were carried out in typical, three-electrode cells comprising flag shaped mild steel coupons, in which an approximately 2 cm² open area was used as the working electrode. The graphite rod and saturated calomel electrode (SCE) were used as auxiliary and reference electrodes, respectively. These electrode cells connected with Autolab potentiostat-galvanostat and computer-controlled NOVA software (version 1.8) were used to record the data. The electrochemical measurements were conducted in aerated, non-stirred 1 M HCl solutions containing different concentrations of inhibitor. Prior to potentiodynamic polarization and impedance measurements, the working electrode was dipped in the test solution until the steady-state open circuit potential (OCP) with respect to the corrosion potential (E_{corr}) was obtained. The potentiodynamic polarization (Tafel plots) was obtained by scanning potential windows of ±250 mV compared to SCE at OCP with a rate of 0.5 mV s⁻¹, and linear polarization resistance (LPR) was obtained from the current versus potential in a range of ±10 mV around E_{corr} . The corrosion current densities (I_{corr}) were obtained from the extrapolated linear region of cathodic and anodic slopes.

The Nyquist and Bode plots with respect to OCP were acquired from EIS analysis using a frequency range of 100 kHz to 50 mHz and 10 mV peak-to-peak amplitude values. The lowest deviated electrochemical equivalent circuit using NOVA software was developed to fit all impedance experimental data.

2.6. Surface Tension Experiments

The PHYWE surface tensiometer (model P2140500, Germany), as described in [39], was utilized to measure the surface tension using du Nouy ring method. The surface tension was calculated from the force on platinum iridium ring—having diameter of 1.88 cm and torsion dynamometer of 0.01 N for tear-off force (at the point of liquid film tears). To measure the surface tension, the different concentrations range 3.75×10^{-6} – 4.50×10^{-4} mol L⁻¹ of corrosion inhibitor 7 were prepared in 1 M HCl at 333 K.

2.7. Surface Analysis

2.7.1. AFM

The surface characteristics of polished, uninhibited, and inhibited mild steel coupons were studied by AFM. The rectangular shaped mild steel coupons, having dimensions of 2.5 cm × 2.0 cm × 0.1 cm, were abraded with different grade sizes (grit size: 100, 600, and 1500) of emery papers, and washed with deionized water and acetone, and dried. For the AFM study, the mild steel coupons were immersed with or without 4.50×10^{-4} mol L⁻¹ of corrosion inhibitor 7 for 6 h in 1 M HCl at 333 K. After the immersion period, the test samples were removed from test solution, washed with de-ionized water and dried in a vacuum oven at 333 K. The AFM images of these mild steel coupons were analyzed using Nanoscope II Atomic Force Microscopy in a tapping mode, by powerful algorithm-containing software (WSxM).

2.7.2. SEM and EDX

The SEM-EDX was utilized to study the change in surface morphology of polished, uninhibited, and inhibited mild steel coupons. The rectangular shaped mild steel coupons of equal sizes (2.5 cm × 2.0 cm × 0.1 cm) were abraded with emery papers (grit size: 100, 600, and 1500), and washed with deionized water and acetone, and dried. For SEM-EDX study, after 6 h immersion of mild steel coupons without or with 4.50×10^{-4} mol L⁻¹ of corrosion inhibitor 7 in 1 M HCl at 333 K, the test samples were removed from test solution, washed with de-ionized water and dried in a vacuum oven at 333 K. The SEM-EDX images were captured by Lyra 3 field-emission scanning electron microscope with speed up voltage of 20–30 kV. The X-Max detector containing EDX spectroscope was employed to determine the chemical compositions and mapping the homogeneity level of these mild steel surfaces.

2.7.3. XPS

The mild steel coupons of equal dimensions (2.5 cm × 2.0 cm × 0.1 cm) were cleaned following the procedure described in earlier sections (SEM-EDX). The mild steel samples were immersed without or with 4.50×10^{-4} mol L⁻¹ of corrosion inhibitor 7 in 1 M HCl at 333 K. After a 6 h immersion, the test samples were removed from test solution, washed with de-ionized water, and dried in a vacuum oven at 333 K. The surface analyses were performed by thermos scientific XPS (Model # 250 Xi, Kansas, MN, USA), and the data were processed by Avantage software (Version 4.88) considering C 1s peak (285.4 eV) as a reference peak. The deconvoluted high resolution XPS spectra were composed by a non-linear least squares Shirley base line and Gaussian–Lorentzian algorithm.

3. Results and Discussion

3.1. Polymers' Syntheses and Characterizations

The homo and co-cyclopolymer of *N,N'*-diallyl-L-methionine hydrochloride and *N,N'*-diallylamino propanephosphonate were prepared using Butler's cyclopolymerization protocol. At the outset, we were apprehensive about the polymerizability of zwitterionic monomer, under free radical conditions in the aqueous solution, readily undergoing cyclopolymerization in the presence of water-soluble free radical initiator AMPD to give zwitterionic polymers 5–7 at very good yields. All the polymers

5–7 were found to be readily soluble in de-ionized water. The intrinsic viscosities of the zwitterionic polymers 5–7 were determined by viscometry using Mark Huggins equation, and the intrinsic viscosity values were found to be 0.098, 0.122, and 0.145 dL g⁻¹, respectively.

The IR spectra of polymers 5–7 were recorded by FT-IR in the frequency range 400–4000 cm⁻¹ (Figure 1). The FT-IR spectra of polymers 5–7 showed that there is a strong absorption peak present around 3425 cm⁻¹ due to the hydrogen bonded N–H group [40]. The symmetric and antisymmetric absorption peaks appearing at ~1455 and ~1458 cm⁻¹, respectively, suggested COO⁻ motifs in the polymers 5 and 7 [36]. The stretching vibration band was found to be absent in polymer 6. The strong absorption bands around 1141 and 1148 cm⁻¹ in polymers 6 and 7, respectively, are associated with the stretching frequency of P=O. The C–N–C motifs in corrosion inhibitors 5–7 were established by the stretching and bending peaks that appeared around 1390 and 775 cm⁻¹, respectively.

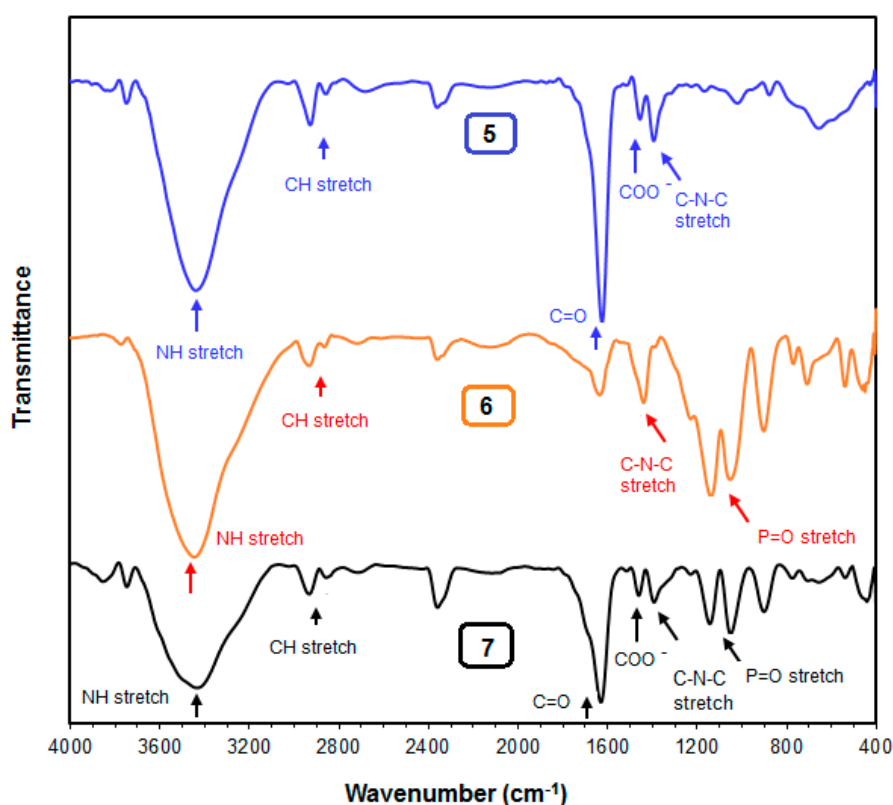


Figure 1. FT-IR spectra for the corrosion inhibitors 5, 6, and 7.

In the NMR spectra, alkene proton and carbon signals in the polymers 5–7 were absent, which indicates that all monomers were converted into polymer. The ¹³C signals around 173 ppm were attributed to the carbonyl groups in the repeating units of 5 and 7. ³¹P NMR signals appeared at 22.1 and 20.9 ppm, respectively, for polymers 6 and 7, which attributed to the higher electron density around P as a result of negatively charged oxygen. The thermal degradation of the polymers was examined by TGA to comprehend the thermal stability of the corrosion inhibitors. The TGA curves of polymers 5–7, presented in Figure 2, showed that without any unexpected weight loss these polymers are stable up to 200 °C. Afterwards, the abrupt weight loss was observed, which might be due to the thermal degradation of the polymers.

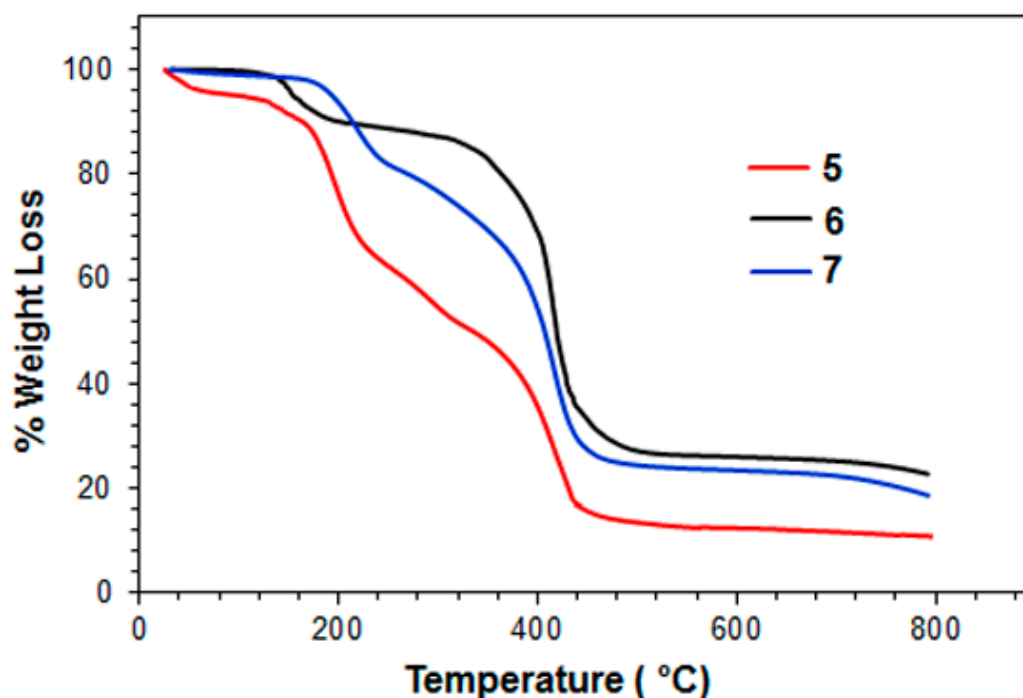


Figure 2. TGA curves for the corrosion inhibitors 5, 6, and 7.

3.2. Corrosion Tests

3.2.1. Gravimetric Weight Loss Measurements

Table 2 presents different corrosion parameters obtained from gravimetric weight loss data using different concentrations (3.75×10^{-6} – 4.50×10^{-4} mol L⁻¹) of corrosion inhibitors 5–7 for mild steel after 6 h immersion in 1 M HCl at different temperature (313–333 K). The inhibition efficiencies ($\eta_1\%$), surface coverage (θ_1) and corrosion rate (CR) were determined by the following Equations (1)–(3):

$$(\eta_1\%) = \left(\frac{\text{Weight loss}_{\text{blank}} - \text{Weight loss}_{\text{inhibitor}}}{\text{Weight loss}_{\text{blank}}} \right) \times 100 \quad (1)$$

$$\theta_1 = \left(\frac{\text{Weight loss}_{\text{blank}} - \text{Weight loss}_{\text{inhibitor}}}{\text{Weight loss}_{\text{blank}}} \right) \quad (2)$$

$$CR \text{ (mmp}^{-1}\text{)} = \left(\frac{8.76 \times 1000 \times W}{D \times A \times t} \right) \quad (3)$$

where W represents weight loss in g, D is the density of mild steel in g cm⁻³, A is the area in cm² of mild steel coupon exposed in solution, and t is the exposure time in h.

Table 2 shows that with increasing the concentration of the corrosion inhibitors 5–7, the corrosion inhibition efficiency increases. These results indicated that by increasing the concentrations of the inhibitors, the mild steel surface coverage increases, which prevents the metal surface from dissolving in acidic media, thereby increasing the inhibition efficiencies [41].

Table 2. Different corrosion parameters: corrosion rate (CR), surface coverage (θ_1), and inhibition efficiency ($\eta_1\%$) of mild steel in 1 M HCl solution without and with corrosion inhibitors 5–7 at different temperatures (313–333 K), obtained from weight loss measurements.

S. Id	Conc. (ppm)	Conc. (mol L ⁻¹)	Temp. (313 K)			Temp. (323 K)			Temp. (333 K)		
			CR (mm y ⁻¹)	θ_1	$\eta_1\%$ ^a	CR (mm y ⁻¹)	θ_1	$\eta_1\%$ ^a	CR (mm y ⁻¹)	θ_1	$\eta_1\%$ ^a
5	0	0	18.6	–	–	33.6	–	–	61.2	–	–
	0.86	3.75×10^{-6}	11.3	0.390	39.0	23.7	0.294	29.4	48.1	0.215	21.5
	4.31	1.88×10^{-5}	9.13	0.509	50.9	17.9	0.466	46.6	41.4	0.323	32.3
	8.60	3.75×10^{-5}	6.94	0.627	62.7	15.7	0.531	53.1	34.7	0.433	43.3
	12.9	5.63×10^{-5}	6.25	0.664	66.4	13.5	0.578	57.8	31.8	0.481	48.1
	25.9	1.13×10^{-4}	5.63	0.697	69.7	11.2	0.656	65.6	27.1	0.558	55.8
	43.1	1.88×10^{-4}	4.46	0.760	76.0	9.52	0.716	71.6	21.2	0.654	65.4
	86.0	3.75×10^{-4}	3.31	0.822	82.2	7.30	0.782	78.2	14.4	0.765	76.5
	103.2	4.50×10^{-4}	2.75	0.852	85.2	6.11	0.818	81.8	12.7	0.793	79.3
6	0.82	3.75×10^{-6}	10.5	0.435	43.5	22.5	0.328	32.8	47.2	0.229	22.9
	4.10	1.88×10^{-5}	8.23	0.558	55.8	17.3	0.483	48.3	36.1	0.411	41.1
	8.19	3.75×10^{-5}	7.46	0.599	59.9	16.2	0.517	51.7	31.6	0.483	48.3
	12.3	5.63×10^{-5}	6.94	0.627	62.7	14.7	0.562	56.2	29.9	0.511	51.1
	24.7	1.13×10^{-4}	5.88	0.684	68.4	12.7	0.622	62.2	26.7	0.564	56.4
	41.1	1.88×10^{-4}	4.99	0.732	73.2	10.9	0.673	67.3	23.2	0.621	62.1
	81.9	3.75×10^{-4}	3.65	0.804	80.4	8.42	0.749	74.9	18.8	0.693	69.3
	98.2	4.50×10^{-4}	3.11	0.833	83.3	7.61	0.773	77.3	16.7	0.727	72.7
7	0.84	3.75×10^{-6}	6.40	0.599	59.9	13.9	0.585	58.5	26.1	0.574	57.4
	4.21	1.88×10^{-5}	4.30	0.694	69.4	9.66	0.712	71.2	20.5	0.665	66.5
	8.19	3.75×10^{-5}	2.72	0.800	80.0	7.07	0.789	78.9	16.6	0.729	72.9
	12.6	5.63×10^{-5}	1.90	0.844	84.4	5.60	0.833	83.3	13.3	0.782	78.2
	25.3	1.13×10^{-4}	0.82	0.902	90.2	3.65	0.891	89.1	9.49	0.845	84.5
	42.1	1.88×10^{-4}	0.39	0.941	94.1	2.54	0.924	92.4	6.31	0.897	89.7
	83.9	3.75×10^{-4}	0.17	0.964	96.4	1.62	0.951	95.1	4.12	0.933	93.3
	100.7	4.50×10^{-4}	0.10	0.995	99.5	0.45	0.985	98.5	1.82	0.978	97.8

^a Triplicate determinations were made in each case using coupons of almost identical masses.

The inhibition efficiency of the studied corrosion inhibitors was found in following order: 7 > 5 > 6. All these three corrosion inhibitors performed as very good inhibitors, but the best performance was obtained by corrosion inhibitor 7. This could be due to the synergistic effect of functional motifs of sulfide, phosphonate, oxide, and quaternary amines that form a layer and inhibit the mild steel corrosion. At 313 K, the inhibition efficiency of corrosion inhibitors 5–7 at $4.50 \times 10^{-4} \text{ mol L}^{-1}$ was found to be 85.2%, 83.3%, and 99.5%, respectively, while at a meager concentration of $1.13 \times 10^{-4} \text{ mol L}^{-1}$ (~25 ppm), the corresponding inhibition efficiency values were calculated to be 69.7%, 68.4%, and 90.2%, respectively (Table 2).

The corrosion inhibition efficiency values of corrosion inhibitors 5–7 was studied in the temperature range 313–333 K. The inhibition efficiency values decreased with increasing the temperature (Table 2). That was explained by the fact that at higher temperature, the dissolution of metals from metal/solution interface could be proliferated, which can aggravate the desorption of adsorbed molecule from the mild steel surface [42]. The corrosion rate of corrosion inhibitor 7 at $4.50 \times 10^{-4} \text{ mol L}^{-1}$ was found superbly low, with values of 0.10, 0.45, and 1.82 mm y^{-1} , respectively, at different temperature of 313, 323, and 333 K (Table 2).

The apparent activation energy (E_a) for mild steel dissolution with and without corrosion inhibitors 5–7 in 1 M HCl was determined by using Arrhenius equation,

$$\log CR = \frac{-E_a}{2.303RT} + \log A \quad (4)$$

where R , T , and A represent the gas constant ($8.314 \text{ J K}^{-1} \text{ mol}^{-1}$), absolute temperature (K), and Arrhenius pre-exponential factor, respectively. The $\log CR$ versus $1/T$ curves have been constructed with and without different concentrations (3.75×10^{-6} – $4.50 \times 10^{-4} \text{ mol L}^{-1}$) of corrosion inhibitors 5–7 in 1 M HCl, and are depicted in Figure 3. The apparent activation energy (E_a) obtained from the slope of Figure 3 are presented in Table 3. The E_a values of different inhibited solutions were found to be higher than those in the uninhibited solution. They could have been due to the fact that, in the presence of corrosion inhibitors, the metal dissolution was decreased due to the formation of a thin layer by adsorption—particularly physisorption of the corrosion inhibitors on mild steel surface [43]. However, Vracar and Drazic [44] indicated that the adsorption types cannot be clearly understood only by the change of activation energy, because a competitive adsorption occurs with water molecules whose removal from the mild steel surface also requires some activation energy. In addition, Ansari et al., suggested that physisorption process usually occurs along with some chemisorption process and vice versa [45].

The standard enthalpy of activation (ΔH^*) and standard entropy of activation (ΔS^*) were determined from Equation (5):

$$CR = \frac{RT}{Nh} e^{\frac{\Delta S^*}{R}} e^{\frac{\Delta H^*}{RT}} \quad (5)$$

where h is the Planck's constant ($6.626 \times 10^{-34} \text{ J sec particle}^{-1}$) and N is the Avogadro number ($6.022 \times 10^{23} \text{ particles mol}^{-1}$), respectively. The $\log (CR/T)$ versus $1/T$ curves have been plotted and presented in Figure 4. The ΔH^* and ΔS^* values were determined from the slope and intercept of Figure 4, and are summarized in Table 3. The corrosion inhibitors 5–7 appeared with negative ΔS^* values, which suggest an decrease in the disorder in the rate determining step at transition from reactants to activated complex [46].

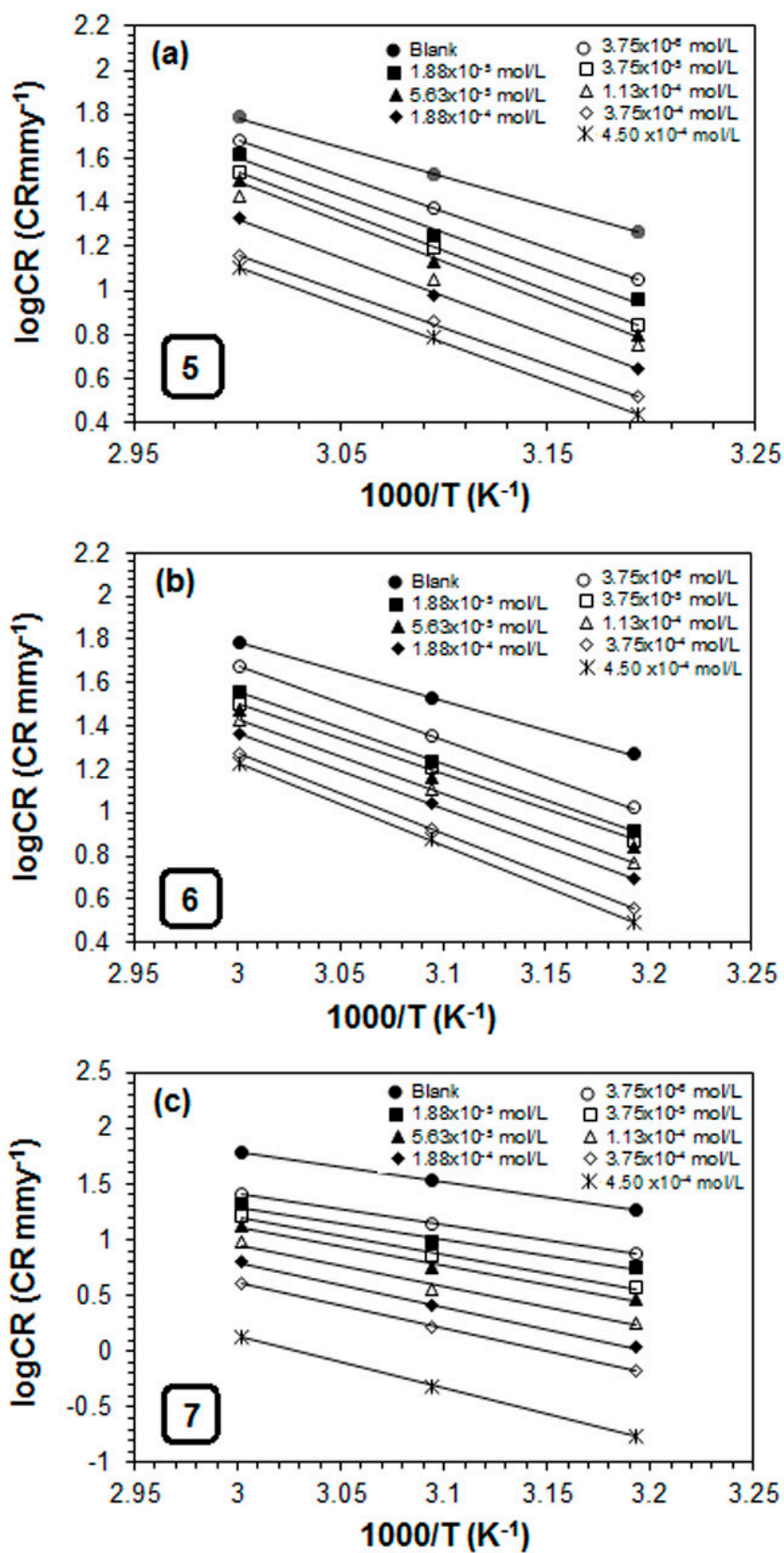


Figure 3. The log CR versus 1000/T curves for mild steel corrosion in a 1 M HCl solution: (a) 5, (b) 6, and (c) 7.

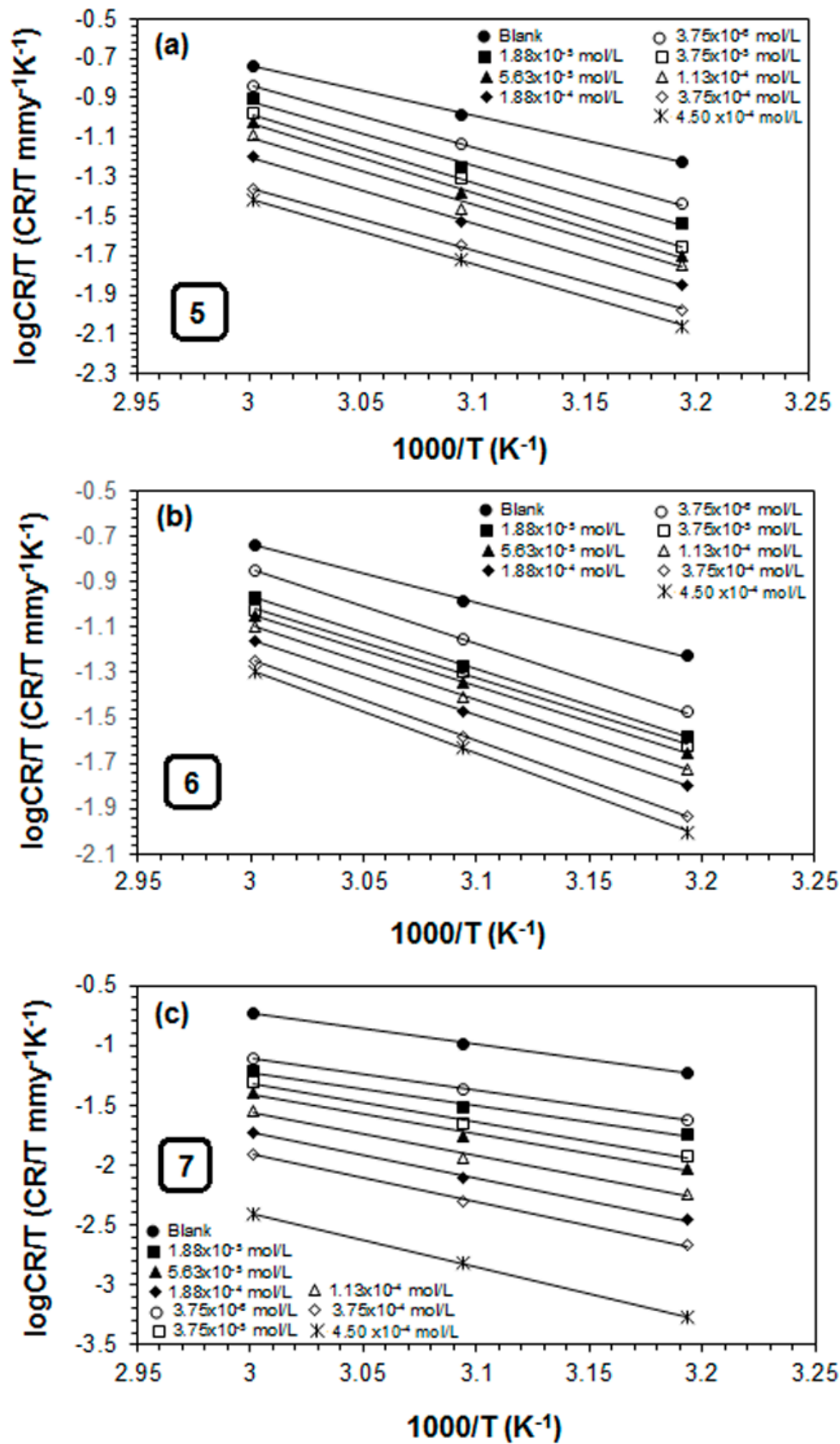


Figure 4. Transition state plot of log CR/T versus 1000/T for mild steel in 1 M HCl solution at different concentrations: (a) 5, (b) 6, and (c) 7.

Table 3. Activation parameters for mild steel in 1 M HCl solution without and with corrosion inhibitors 5–7 obtained from gravimetric weight loss measurements.

Sample	Conc. (ppm)	Conc. (mol L ⁻¹)	E _a (kJ mol ⁻¹)	ΔH° (kJ mol ⁻¹)	ΔS° (kJ mol ⁻¹ K ⁻¹)
5	0	0	51.6	48.9	−64.8
	0.86	3.75 × 10 ⁻⁶	62.6	59.9	−33.8
	4.31	1.88 × 10 ⁻⁵	63.8	62.8	−26.7
	8.60	3.75 × 10 ⁻⁵	65.5	67.1	−14.9
	12.9	5.63 × 10 ⁻⁵	67.5	67.8	−13.8
	25.9	1.13 × 10 ⁻⁴	68.0	65.3	−22.8
	43.1	1.88 × 10 ⁻⁴	69.8	64.8	−25.9
	86.0	3.75 × 10 ⁻⁴	70.5	61.1	−40.1
	103.2	4.50 × 10 ⁻⁴	66.4	63.7	−33.5
6	0.82	3.75 × 10 ⁻⁶	62.7	62.4	−26.4
	4.10	1.88 × 10 ⁻⁵	63.4	61.4	−31.8
	8.19	3.75 × 10 ⁻⁵	64.1	60.0	−36.9
	12.3	5.63 × 10 ⁻⁵	65.1	60.7	−35.4
	24.7	1.13 × 10 ⁻⁴	65.6	62.9	−29.7
	41.1	1.88 × 10 ⁻⁴	66.7	64.0	−27.6
	81.9	3.75 × 10 ⁻⁴	71.1	68.4	−16.1
	98.2	4.50 × 10 ⁻⁴	73.1	70.4	−11.0
7	0.84	3.75 × 10 ⁻⁶	54.3	51.6	−63.9
	4.21	1.88 × 10 ⁻⁵	55.4	52.7	−62.8
	8.19	3.75 × 10 ⁻⁵	64.7	62.0	−36.7
	12.6	5.63 × 10 ⁻⁵	66.1	63.4	−34.2
	25.3	1.13 × 10 ⁻⁴	71.5	68.8	−21.0
	42.1	1.88 × 10 ⁻⁴	76.1	73.4	−10.5
	83.9	3.75 × 10 ⁻⁴	78.9	76.2	−5.36
	100.7	4.50 × 10 ⁻⁴	87.9	86.1	−0.17

3.2.2. Adsorption Isotherms

An adsorption isotherm provides the inhibitive pattern of corrosion inhibitors on their adsorption behavior onto the metal surface. The inhibition efficiency (η_1) of the corrosion inhibitors 5–7 were determined to realize the surface coverage (θ_1) of mild steel. The $\eta_1\%$ and θ_1 values are reported in Table 2. The corrosion inhibitor 7 provided the best protection in all studied conditions. Therefore, in the subsequent discussions, we mainly concentrate to explore the inhibitive effect of corrosion inhibitor 7 in acidic media. In order to understand the adsorption mechanism of the best performing corrosion inhibitor 7, several commonly used adsorption isotherm models, such as those of Freundlich, Langmuir, Frumkin, and Temkin (Equations (6)–(9)) analyzed the inhibitor's adsorption thermodynamics.

$$\text{Freundlich: } \theta = K_{\text{ads}} C^n \quad (6)$$

$$\text{Langmuir: } \theta/(1-\theta) = K_{\text{ads}} C \quad (7)$$

$$\text{Frumkin: } K_{\text{ads}} C = \{\theta/(1-\theta)\} e^{-2\alpha\theta} \quad (8)$$

$$\text{Temkin: } K_{\text{ads}} C = e^{f\theta} \quad (9)$$

where K_{ads} is the adsorption–desorption equilibrium constant, n is the Freundlich adsorption intensity, and α and f are the Frumkin and Temkin adsorbate parameters, respectively.

The correlation between the surface coverage (θ) and the bulk low concentration of inhibitor (C) was established by the linear least square method [47]. The square correlation coefficients (R^2) and the values of the different constants obtained from different isotherms for corrosion inhibitor 7 at different temperatures are presented in Table 4. The plots of $\theta/(1 - \theta)$ versus C yielded straight lines (Figure 5)

with square correlation coefficients (R^2) very close to 1 for synthesized corrosion inhibitor 7 in 1 M HCl at different temperatures (313–333 K), as presented in Table 4, suggesting that the Langmuir adsorption isotherms fitted very well to explain the adsorption behavior of corrosion inhibitor 7 on the metal surface (Figure 5).

Table 4. Adsorption parameters for corrosion inhibitor 7 calculated from Langmuir adsorption isotherm, and the square correlation coefficient (R^2) and constant values in different adsorption isotherms for mild steel in 1 M HCl solution at different temperatures.

Temp. (K)	Langmuir			Temkin	Frumkin	Freundlich
	K_{ads} ($L mol^{-1}$)	ΔG° ($kJ mol^{-1}$)	R^2	(R^2, f)	(R^2, a)	(R^2, n)
313	8.00×10^4	−39.8	0.9963	0.9727, 9.52	0.9279, −0.79	0.9808, 0.1
323	5.71×10^4	−38.9	0.9982	0.9863, 11.9	0.9819, −1.8	0.9917, 0.1
333	3.93×10^4	−37.9	0.9975	0.9879, 10.8	0.9667, −1.8	0.9910, 0.1

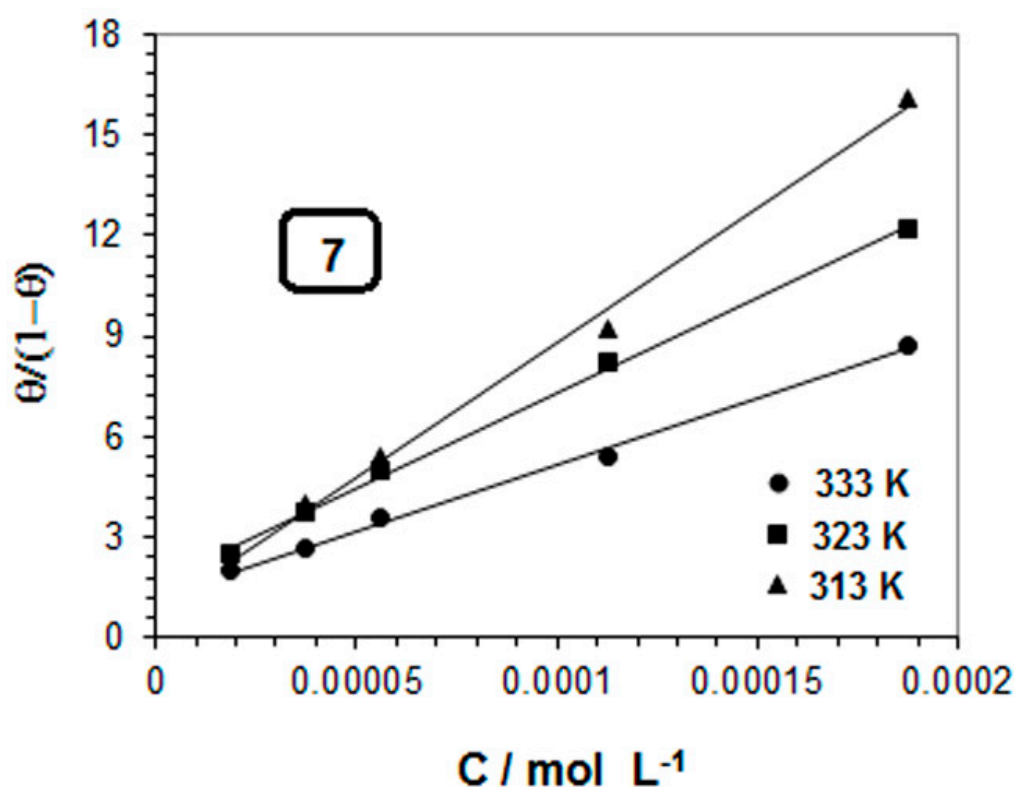


Figure 5. Langmuir adsorption isotherm for the corrosion inhibitor 7 in 1 M HCl at 313–333 K.

The adsorption mechanism was further investigated using various thermodynamic parameters, such as adsorption equilibrium constant (K_{ads}), and the standard free energy of adsorption (ΔG°_{ads}). K_{ads} values were calculated from the slopes of the straight lines obtained from Langmuir adsorption isotherms (Figure 5), and the standard free energy of adsorption (ΔG°_{ads}) values were obtained from Equation (10).

$$K_{ads} = \frac{1}{55.5} e^{\frac{-\Delta G^{\circ}_{ads}}{RT}} \quad (10)$$

The K_{ads} and ΔG°_{ads} values are presented in Table 4.

In general, the mechanism of adsorption can be categorized by the magnitude of ΔG°_{ads} as a form of physisorption or chemisorption or mixed mechanism. When the absolute value of ΔG°_{ads} is

up to -20 kJ mol^{-1} , the adsorption process is classified as physisorption. The physisorption usually arises due to electrostatic interactions between corrosion inhibitors and the charged metal surface. When the absolute value of $\Delta G^{\circ}_{\text{ads}}$ is more negative than -40 kJ mol^{-1} , the adsorption process is classified as chemisorption. In the chemisorption process, the inhibitor molecules share and/or transfer the charges to the metal surface in order to form a coordinate type metallic bond. When $\Delta G^{\circ}_{\text{ads}}$ values falls between -20 kJ mol^{-1} and -40 kJ mol^{-1} , the adsorption process is, in general, considered a mixed mechanism [48]. The $\Delta G^{\circ}_{\text{ads}}$ values of the synthesized corrosion inhibitor 7 (Table 4) at different temperatures (313–333 K) were found in the range of (-37.9 to $-39.8 \text{ kJ mol}^{-1}$), which are far more negative than -20 kJ mol^{-1} but only slightly less negative than -40 kJ mol^{-1} . These results indicate that the adsorption process might occur due to mixed mechanism (physisorption and chemisorption). Though it is very difficult to conclude the adsorption process solely based on $\Delta G^{\circ}_{\text{ads}}$ values, the reported values in this work suggests that it is predominantly influence by the chemisorption process [49].

3.2.3. Electrochemical Studies

Prior to the electrochemical analysis, the steady state OCP values were determined by immersing the mild steel electrode in 1 M HCl. To obtain a stable OCP, the mild steel electrode was immersed without and with corrosion inhibitor 7 at two different concentrations (1.88×10^{-5} and $4.50 \times 10^{-4} \text{ mol L}^{-1}$) for different span of time (0–60 min.) at 333 K. It was found that E_{corr} becomes almost unchanged after 25 min of immersion, which is indicative of the steady state. Therefore, in all subsequent electrochemical experiments, the mild steel electrode was immersed in the test solution for 30 min before recording the data.

Potentiodynamic Polarization Study

The Tafel extrapolation curves were plotted for the mild steel without and with corrosion inhibitor 7 at different concentrations (3.75×10^{-6} – $4.50 \times 10^{-4} \text{ mol L}^{-1}$) in 1 M HCl solution at 333 K, and depicted in Figure 6. The various corrosion parameters, such as corrosion potential (E_{corr}), anodic Tafel slope (β_a), cathodic Tafel slope (β_c), and corrosion current density (I_{corr}) were obtained from Tafel extrapolation curves, and are presented in Table 5.

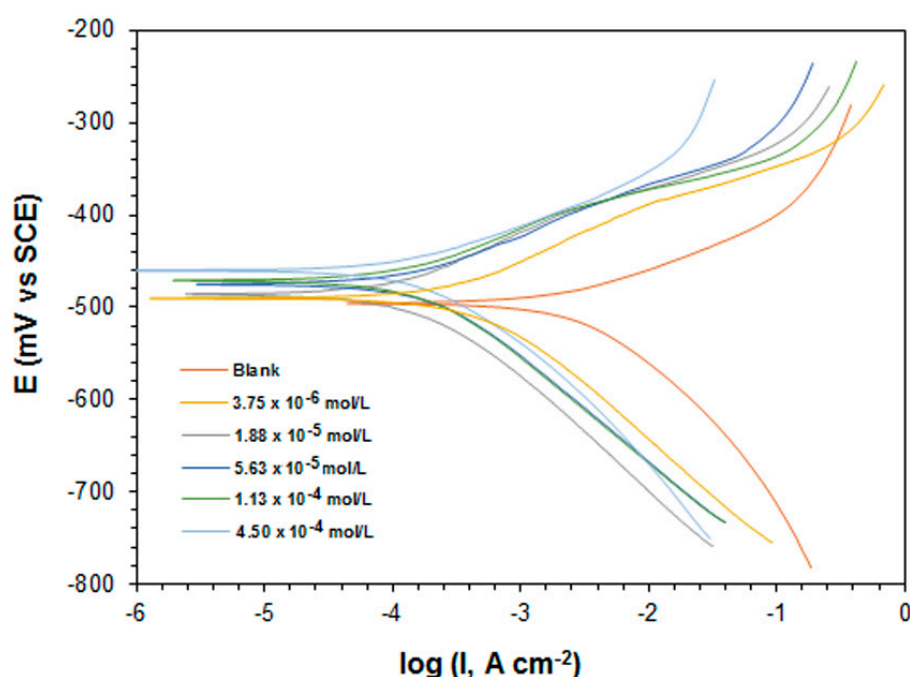


Figure 6. Tafel plots for mild steel in 1 M HCl solution without and with corrosion inhibitor 7 at 333 K.

Table 5. Electrochemical results of Tafel plots and LPR of a mild steel sample in 1 M HCl containing corrosion inhibitor 7 at 333 K.

Conc. (ppm)	Conc. (mol L ⁻¹)	Tafel				LPR ^b	
		E _{corr} vs. SCE (mV)	β _a (mV dec ⁻¹)	β _c (mV dec ⁻¹)	I _{corr} ^c (μA cm ⁻²)	η ₂ (%) ^a	θ ₂ (%) ^a
0	0	-495	73.8	-169	2465	–	–
0.84	3.75 × 10 ⁻⁶	-490	129	-124	1129	54.2	55.7
4.21	1.88 × 10 ⁻⁵	-486	121	-183	939	61.9	62.3
8.19	3.75 × 10 ⁻⁵	-481	108	-137	781	68.3	69.4
12.6	5.63 × 10 ⁻⁵	-475	80.3	-125	680	72.4	71.9
25.3	1.13 × 10 ⁻⁴	-470	79.1	-115	468	81.0	81.8
42.1	1.88 × 10 ⁻⁴	-463	58.6	-113	355	85.6	87.1
83.9	3.75 × 10 ⁻⁴	-461	62.2	-110	244	90.1	92.3
100.7	4.50 × 10 ⁻⁴	-459	47.9	-119	96.1	94.7	96.1

^a Inhibition efficiency (η₂); surface coverage (θ₂); ^b Polarization resistance for blank at 333 K: 2.38 Ω · cm²; ^c Triplicate determinations were made, and the standard deviation of I_{corr} data varied the range of 0.5–2.4%.

The percentage inhibition efficiency (η₂%) based on I_{corr} was calculated using Equation (11).

$$(\eta_2\%) = \left(\frac{I_{\text{blank}} - I_{\text{inhibitor}}}{I_{\text{blank}}} \right) \times 100 \quad (11)$$

where, I_{blank} and I_{Inhibitor} represent the corrosion current densities with and without corrosion inhibitor, respectively.

The surface coverage (θ₂) was determined from linear polarization resistance without (R_p) and with (R'_p) corrosion inhibitor by Equation (12).

$$\theta_2(\%) = \left(\frac{R'_p - R_p}{R'_p} \right) \times 100 \quad (12)$$

The inhibitive nature of the synthesized polymers was indicated by the significant decrease in the I_{corr} values. Figure 6 shows that with increasing the concentrations of corrosion inhibitor, the anodic (metal dissolution) and cathodic (hydrogen evolution) slope in the Tafel plots shifted towards lower I_{corr}. With increasing the concentrations of corrosion inhibitor 7, decreasing the I_{corr} values suggested that corrosion inhibitors diminished the corrosion reaction on the mild steel surface by the adsorption process, thereby increasing the inhibition efficiency [50].

The β_a and β_c changes with increasing concentrations of corrosion inhibitor 7 suggested that this inhibitor could control both anodic and cathodic reactions, thus its being considered a mixed type inhibitor. Several research studies reported that if the variation of E_{corr} value in the presence of corrosion inhibitor is >85 mV, then the corrosion inhibitor is considered to be a cathodic or anodic type inhibitor. On the other hand, if the variation of E_{corr} value in the presence of corrosion inhibitor is <85 mV, then the corrosion inhibitor would be considered a mixed type inhibitor [18,40,51]. In this study, the maximum shift in E_{corr} was found to be 36 mV towards the anodic direction, indicating that the corrosion inhibitor cannot solely be classified as anodic type inhibitor but can be recognized as a mixed type inhibitor. It is worth mentioning here that some of the anodic polarization curves appeared with slight desorption potentials (Figure 6). It could be explained by the fact that at a lower potential, the corrosion inhibitor is confined in the anodic sites, and later, at a higher potential, the corrosion inhibitor desorbs, which could lead to an enhancement of the dissolution of metal.

EIS Study

To better understand the corrosion inhibition mechanism and adsorption phenomena, the EIS measurements were carried out after 30 min immersion at the mild steel and 1 M HCl solution interface

with and without different concentrations (3.75×10^{-6} – 4.50×10^{-4} mol L⁻¹) of corrosion inhibitor 7 at 333 K. The recorded Nyquist and Bode plots of mild steel sample–solution interface are shown in Figure 7.

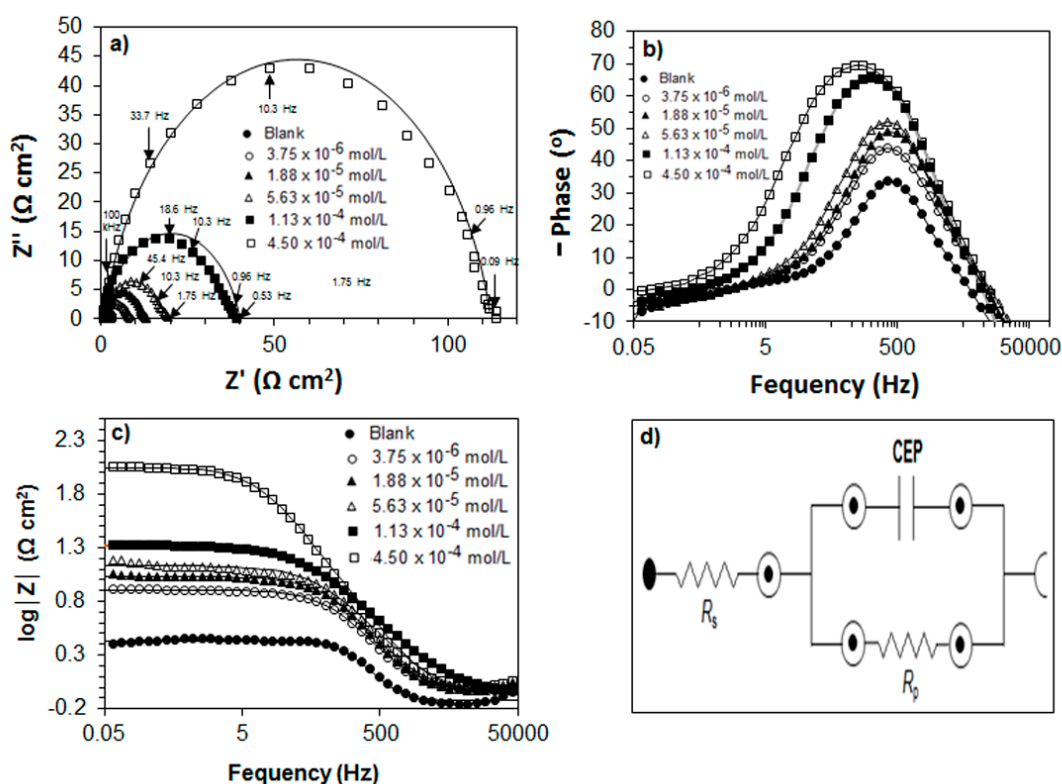


Figure 7. (a) Nyquist plots, (b) Bode phase angle plots, (c) Bode plots of mild steel at 333 K in 1 M HCl containing different concentrations of corrosion inhibitors 7, and (d) the equivalent circuit model used to fit the electrochemical impedance spectroscopy (EIS) data. The solid line in the Nyquist plot is fitted to the equivalent circuit; various symbols represent experimental data and solid lines represent fitted data.

The Nyquist plots (Figure 7a) showed a depressed semi-circle in the first quadrant that suggests one time-constant involved in the charge transfer process, thus the capacitor at the inhibitor solution and metal interface does not behave as a real capacitor [43]. Moreover, the non-ideal or depressed semicircle in the Nyquist plots are attributed to a phenomenon called “dispersing effect” associated with the roughness and inhomogeneity of mild steel surface due to the adsorption of corrosion inhibitors or the generation of defects [52]. In the Nyquist plot, shown in Figure 7a, the inhibited solution provided a larger diameter of the capacitive loop than the uninhibited solution, which clearly indicates the formation of a protective layer on the mild steel surface due to the adsorption of the corrosion inhibitor 7.

The EIS data were analyzed by an equivalent circuit, which consisted of a solution resistance (R_s), polarization resistance (R_p), and a constant phase element (CPE), which is shown in Figure 7d. The R_s and R_p values were determined following the procedure as described [40], and used in Equation (13) to calculate the net polarization resistance (R'_p).

$$R'_p = R_p - R_s \quad (13)$$

The $\eta_3\%$ was then determined from net polarization resistance without (R_p) and with (R'_p) corrosion inhibitor by Equation (14).

$$\eta_3(\%) = \left(\frac{R'_p - R_p}{R'_p} \right) \times 100 \quad (14)$$

Several reports have been published for which a similar kind of electrochemical circuit was used to model the iron-acid interface [39,40,53]. The impedance parameters obtained from the equivalent circuit are given in Table 6. The constant phase element (CPE) used in EIS system to express the non-ideal capacitance and non-ideal frequency response in the electrochemical circuit related to n in the software simulation for better fitting the equivalent circuit. The double layer capacitance (C_{dl}) was calculated by Equation (15).

$$C_{dl} = \text{CPE}(\omega)^{n-1} \quad (15)$$

where ω is the angular frequency (radian) at the highest imaginary part of the impedance, and n is the CPE exponent, which represents the surface heterogeneity and its value varies between 0 to 1.

Table 6. Impedance parameters for the corrosion of a mild steel sample in 1 M HCl solutions containing corrosion inhibitor 7 at 333 K.

Conc. (ppm)	Conc. (mol L ⁻¹)	R_s (Ω cm ²)	R_p (Ω cm ²)	CPE ^a (μ F cm ⁻²)	n	R'_p (Ω cm ²)	$\eta_3(\%)$
0	0	0.373	1.963	922	0.989	1.590	–
0.84	3.75×10^{-6}	0.372	3.994	520	0.956	3.622	56.1
4.21	1.88×10^{-5}	0.325	4.729	485	0.912	4.404	63.9
8.19	3.75×10^{-5}	0.268	5.732	479	0.905	5.464	70.9
12.6	5.63×10^{-5}	0.181	7.223	468	0.881	7.042	77.4
25.3	1.13×10^{-4}	0.145	9.553	457	0.857	9.408	83.1
42.1	1.88×10^{-4}	0.138	12.86	476	0.812	12.72	87.5
83.9	3.75×10^{-4}	0.362	22.76	416	0.805	22.39	92.9
100.7	4.50×10^{-4}	0.238	36.38	409	0.783	36.14	95.6

^a Double layer capacitance (C_{dl}) and coating capacitance (C_c) are usually modelled with a constant phase element (CPE) in modeling an electrochemical phenomenon.

Table 6 shows that R'_p values increased and CPE values decreased with increasing inhibitor concentrations, suggesting a decrease in the local dielectric constant and/or an increase in the thickness of the electrical double layer, by an adsorption of corrosion inhibitor 7 at the metal-solution interface that eventually helps to increase the inhibition efficiency (Table 6) [54]. The n values were found to be less than 1 and decreased with increasing the inhibitor concentrations attributed to an increase in the heterogeneity of the metal surface.

The Bode plots for mild steel without and with different concentrations (3.75×10^{-6} – 4.50×10^{-4} mol L⁻¹) of corrosion inhibitor 7 are shown in Figure 7b,c. From the Bode phase angle plot (Figure 7b) for corrosion inhibitor 7, the single-phase peak close to -90° observed at the intermediate frequency range suggested there was a time constant which helped increase the thickness of electrical double layer formation at the metal-solution interface [53]. In addition, it was found that with an increase in the concentration of corrosion inhibitors, the diameter of the high frequency loop increases, which suggests a decrease in the local dielectric constant and an increase in the surface coverage of mild steel samples [55]. The Bode magnitude plots showed, in Figure 7c, that the Z value increased with the increasing concentration of corrosion inhibitor 7. This was attributed to the fact that the corrosion rate was decreased in the presence of corrosion inhibitor, and continued to decrease with an increasing concentration of inhibitor.

The inhibition efficiency obtained from the electrochemical impedance method (Table 6) followed similar trend as those obtained from gravimetric weight loss (Table 2) and potentiodynamic polarization methods (Table 5).

3.3. Surface Tension

The surface tension and critical micelle concentration (CMC) value of the corrosion inhibitor 7 were determined by surface tensiometer in 1 M HCl solution at 333 K. Using the individual CMC values, the standard Gibbs free energy of micelle formation (ΔG°_{mic}) was determined by Equation (16).

$$\Delta G^{\circ}_{mic} = RT \ln(C_{cmc}), \quad (16)$$

where C_{cmc} stands for critical micelle concentration of corrosion inhibitor in mol L^{-1} .

The surface tension versus concentration curve for the corrosion inhibitor 7 is shown in Figure 8a. The adsorption process was realized by measuring the surface tension of the corrosion inhibitor for micellization. The CMC value of corrosion inhibitor 7 was found to be $98.4 \times 10^{-6} \text{ mol L}^{-1}$. At the critical micelle concentration, the inhibition efficiency value obtained from different techniques (Figure 8b) was found to be $\approx 80\%$. The results suggested that the corrosion inhibitor 7 formed a thin film barrier and covered most of the mild steel surface before the concentration reached to its CMC, after which the micelles can help form a multilayered film that could offer additional protection to the metal surface.

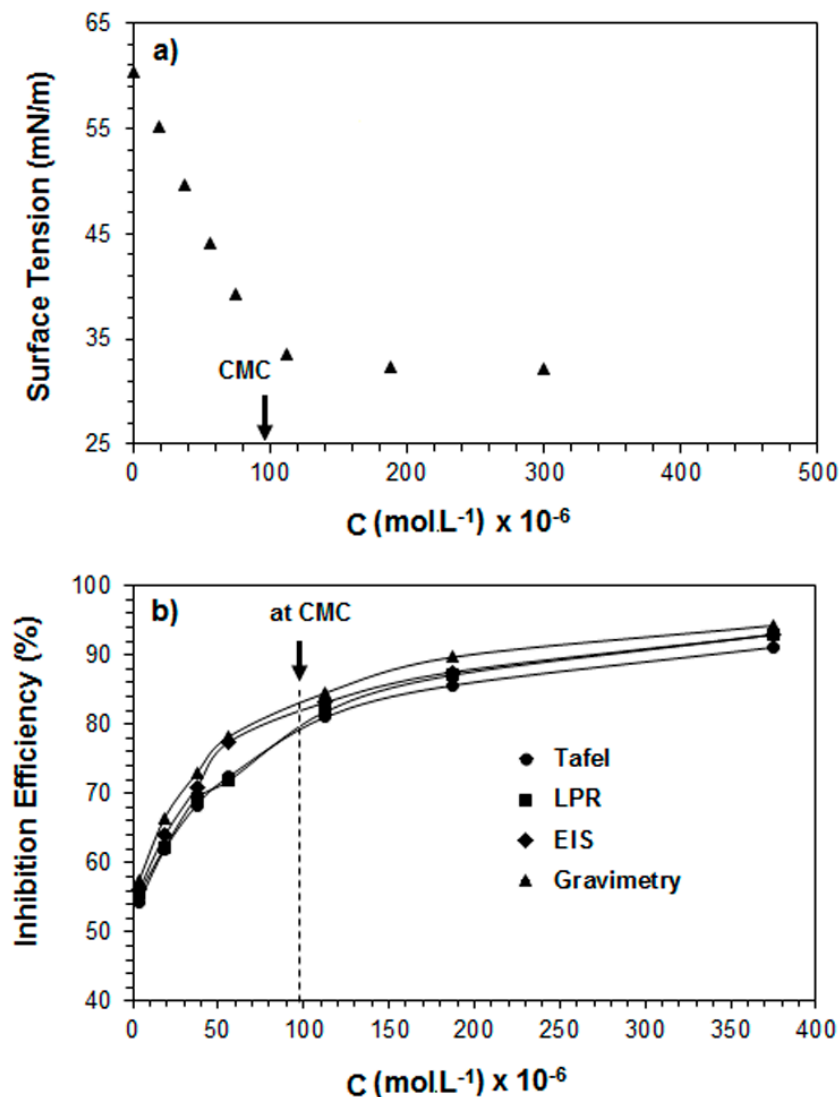


Figure 8. (a) Surface tension versus concentration, and (b) inhibition efficiency versus concentrations of corrosion inhibitor 7 in 1 M HCl at 333 K.

3.4. Surface Analysis

To confirm the effectiveness of corrosion inhibitors, AFM, SEM-EDX, and XPS were used to analyze the surface morphology of the mild steel with and without corrosion inhibitor 7.

Figure 9a shows the AFM surface topologies of polished mild steel surface. The average surface roughness of the polished surface was found to be 15.2 nm. The slight roughness appeared on the polished mild steel surface could be either due to the inherent properties of metal and/or atmospheric corrosion. Figure 9b shows the pitted and corroded mild steel surface in absence of corrosion inhibitors in 1 M HCl. It was found that the metal surface was severely damaged and the average surface roughness was increased to 284 nm. These data suggest that the mild steel surface exposed in 1 M HCl has a greater surface roughness than the polished mild steel surface. The bigger surface roughness of mild steel could be due to the corrosion in acidic environment. Figure 9c shows the mild steel surface exposed in 1 M HCl in presence of corrosion inhibitor 7 at a concentration of $4.50 \times 10^{-4} \text{ mol L}^{-1}$. The average surface roughness was reduced to 6 nm, which is considerably less than in uninhibited environment. The relatively smoother surface is due to the formation of a protective film by adsorption of corrosion inhibitor 7 on the metal surface, thereby efficiently inhibited the corrosion of mild steel sample [56].

Figure 9d depicts the SEM surface morphology of the reference (polished) mild steel, which is relatively smooth (Figure 9d). After immersion of mild steel in absence of corrosion inhibitor 7 in 1 M HCl, the surface becomes very rough, porous, and severely damaged in comparison to the polished surface. This could be due to the dissolution of metal by the exposure to acid. However, in the presence of $4.50 \times 10^{-4} \text{ mol L}^{-1}$ of corrosion inhibitor 7, the damage of the mild steel surface is significantly reduced (Figure 9f) compared to the uninhibited surface immersed in acid solution (Figure 9e). These results suggest that the corrosion inhibitor forms a protective inhibitor film on the metal surface by reducing the contact between the metal surface and acid solution, and reduces the rate of corrosion. The EDX spectra of polished mild steel sample appeared with a strong iron signal, presented in Figure 10a. In Figure 10b, the presence of iron and oxygen signal is an indication of slow atmospheric oxidation in acidic media. On the other hand, the EDX spectra of an inhibited mild steel sample showed a decreased intensity signal of iron (Figure 10c) in comparison with a polished and uninhibited mild steel sample. Moreover, additional signals of carbon, oxygen, nitrogen, phosphorous, and sulfur appeared on the inhibited mild steel sample. The decreased iron signal is due to the inhibitory effect of corrosion inhibitor 7 adsorbed on the metal surface, forming a protective layer between the metal surface and acid solution, and safeguarded the mild steel surface from corrosion attack.

The XPS survey scan of the surface of the mild steel coupons after immersion in 1M HCl containing corrosion inhibitor 7 shows high carbon and small Fe, and significant amounts of N, S, and P content confirm the presence of a carbonaceous polymeric film containing N, S, and P on the mild steel surface (Table 7). The wide scan XPS survey spectra of inhibited mild steel surface indicated the presence of corrosion inhibitor (Figure 11a).

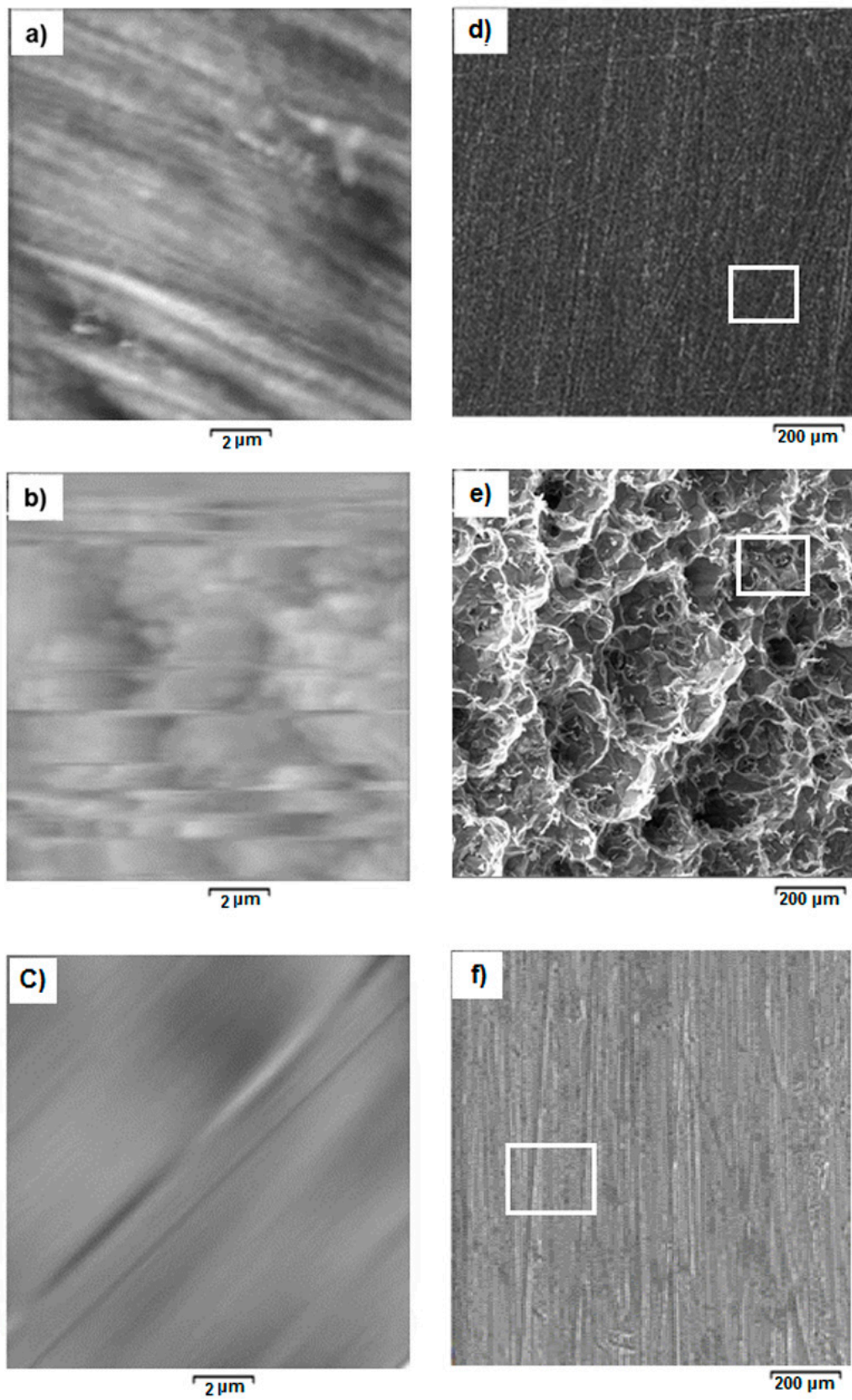


Figure 9. AFM surface topologies and SEM images of mild steel surfaces in 1 M HCl at 333 K: (a,d) polished before immersion, (b,e) immersion blank (uninhibited), and (c,f) immersion in the presence of $4.50 \times 10^{-4} \text{ mol L}^{-1}$ corrosion inhibitor 7.

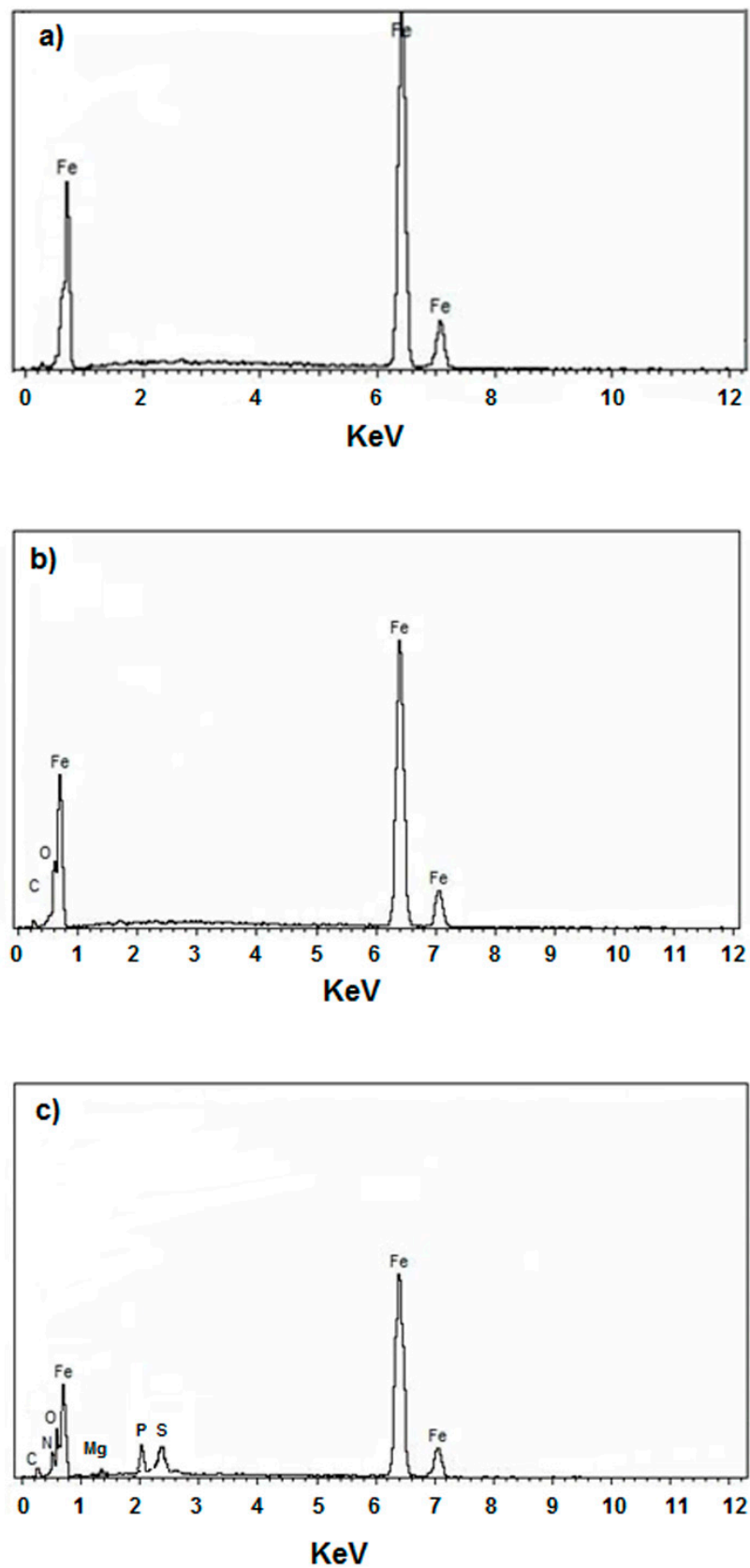
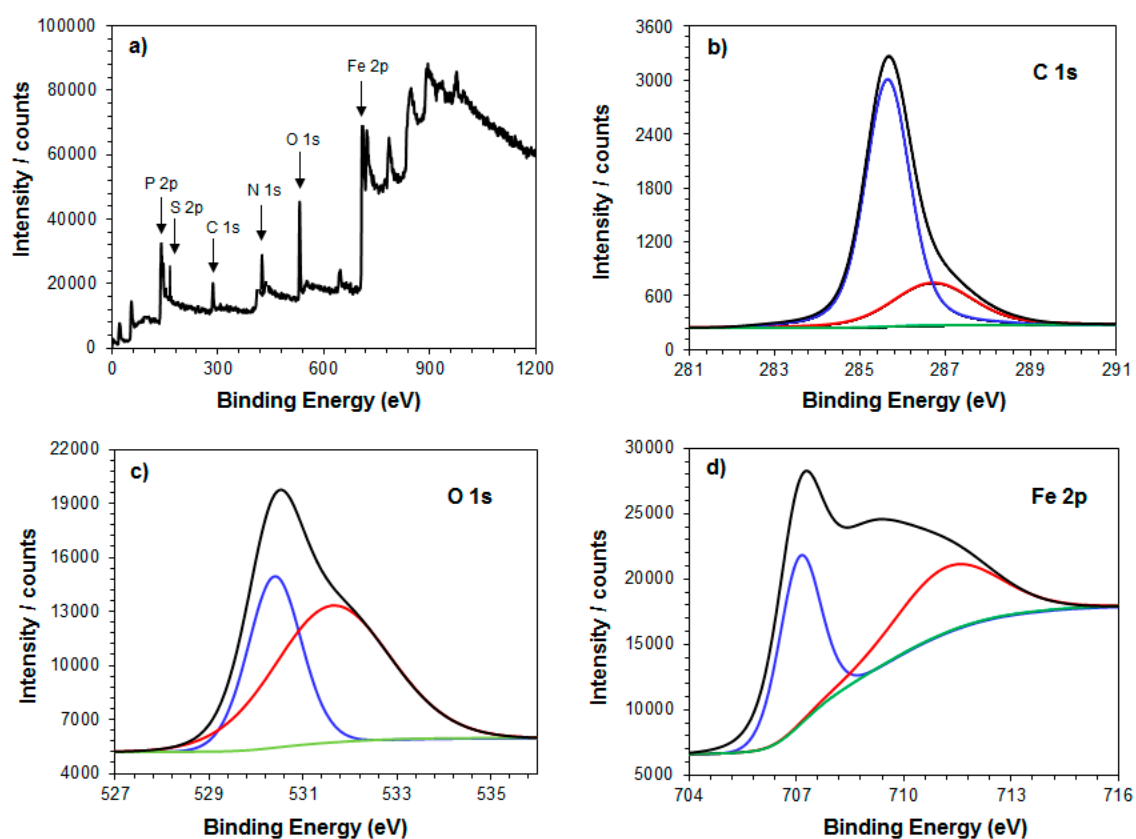


Figure 10. EDX spectra of white, marked areas of (a) polished, (b) uninhibited (blank), and (c) inhibited (4.50×10^{-4} mol L⁻¹ corrosion inhibitor 7) mild steel samples.

Table 7. XPS scan composition of Fe immersed in inhibited solution of 1 M HCl at 333 K for 6 h.

Peak	Approx. Binding Energy (eV)	Composition (Atom %)
C1s	285.3	20.7
C1s	286.5	35.8
O 1s	530.3	4.15
O 1s	532.7	23.9
N 1s	401.1	3.12
Fe 2p	707.1	0.59
Fe 2p	712.2	2.01
S 2p	162.3	4.58
P 2p	133.7	5.12

**Figure 11.** (a) Wide scan XPS spectra of Fe, and XPS deconvoluted spectra of (b) C 1s, (c) O 1s, and (d) Fe 2p in the presence of 4.50×10^{-4} mol L⁻¹ of corrosion inhibitor 7 after immersion of mild steel in 1 M HCl at 333 K for 6 h.

The deconvoluted (high resolution) XPS spectra for the C 1s, O 1s, and Fe 2p signals of film coated mild steel samples are shown in Figure 11b–d, respectively. The deconvoluted C 1s spectra (Figure 11b) showed two-peak profile at 285.3 eV and 286.5 eV, respectively. The peak at 285.3 eV was assigned to the C–C aliphatic bonds, while the presence of C=C, C=O, and C–N bonds were reflected by the peak at 286.5 eV [57]. The presence of O 1s peak at 530.3 eV, shown in Figure 12, is attributed to C–O and O²⁻, and the peak appearing at 532.7 eV could be associated with the oxygen of adsorbed water [49]. The signal that appeared at 712.2 eV corresponds to the ferric compounds, such as FeOOH and Fe₂O₃ (i.e., Fe³⁺ oxide), and the signal at 707.1 eV was attributed to the presence of Fe⁰ (2p) (Figure 11d) [58]. It is worth mentioning that the sulfide peak usually appears at 162.3 eV [40], and the signal at 133.7 eV corresponds to the P–O group present in the inhibitor molecule [57].

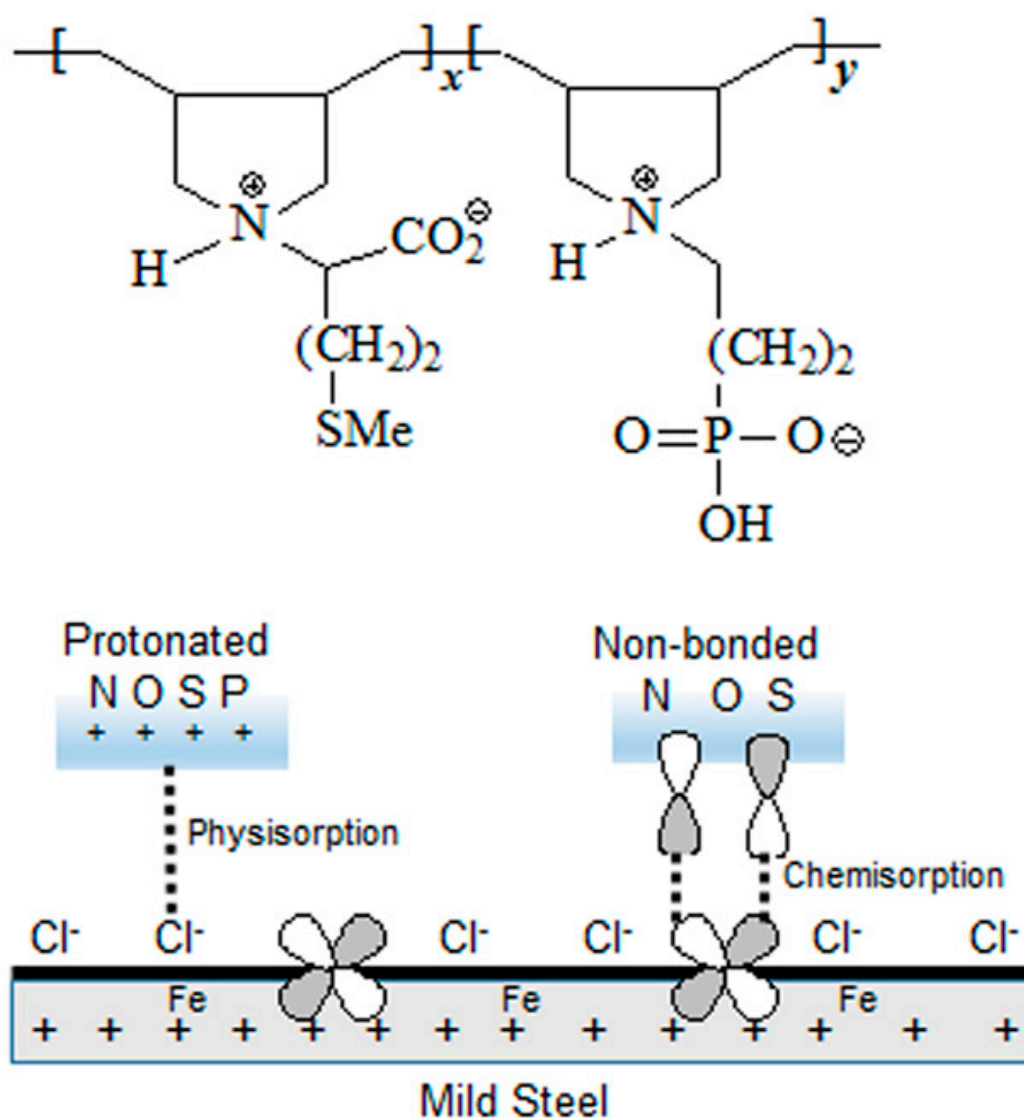


Figure 12. The schematic adsorption mechanism of corrosion inhibitors.

3.5. Mechanism of Inhibition

The adsorption phenomena of corrosion inhibitors on mild steel surface in acidic (1 M HCl) media can be explained by molecular adsorption considering physisorption, chemisorption, or a mixed mechanism. The adsorption process follows physisorption, when the corrosion inhibitors adsorb on the mild steel surface via an electrostatic interaction between the protonated corrosion inhibitors and the charged mild steel metal surface. The chemisorption of corrosion inhibitors arises due to charge sharing or charge transfer (donor–acceptor) between the lone pair of electrons present in the inhibitors and vacant d orbitals of Fe [59]. In this study, the Gibbs free energies of adsorption of the studied inhibitor were found in the range of -37.9 to -39.8 kJ mol^{-1} (Table 4), which indicates that the adsorption mechanism of corrosion inhibitors on the mild steel surface follow a mixture of both physisorption and chemisorption process. In addition, the apparent activation energy (Table 3) results suggest that the corrosion inhibitors are adsorbed on the metal surface by both physisorption and chemisorption processes.

The corrosion inhibitor controls anodic and cathodic reactions to inhibit the corrosion on the metal surface. The E_{corr} values of mild steel sample shifted to 36 mV, towards anodic direction, suggesting the corrosion inhibitor could be classified as mixed type inhibitor (Table 5; Figure 6).

The heteroatoms play a significant role in the adsorption process of inhibitor molecules onto the mild steel surface (Figure 12). Due to the unshared pair of electrons, the heteroatoms N, O, S, and P containing inhibitor molecules can easily be protonated in strong corrosive electrolyte (HCl, H₂SO₄, HNO₃, and H₃PO₄) solution [26,27]. Therefore, the corrosion inhibitors studied in this paper exist as protonated species in 1 M HCl solution [60]. In the case of adsorption of protonated inhibitor molecules, it is well known that the mild steel surface carries positive charge in acidic media [61]; therefore, due to the electrostatic repulsion, the protonated corrosion inhibitor and positively charged H₃O⁺/metal interface cannot easily approach each other. As a consequence, chloride ions, as counterions of corrosive electrolytes, having a smaller degree of hydration, provide excess negative charge to the interface, that results in a negatively charged metallic surface. Subsequently, the negatively charged metal interface is electrostatically attracted to the protonated (positively charged) corrosion inhibitors, and the behavior of inhibitors on metallic surface initially obeys the physisorption mechanism (Figure 12) [62,63]. However, during the metal inhibitor interactions, the non-bonding electrons of heteroatoms are transferred by charge donation into the d orbital of the Fe surface, which results in the formation of coordinate bond (chemisorption) between inhibitor molecules and the metal's surface (Figure 12) [64]. In this study, the protonated corrosion inhibitors were adsorbed on to the cathodic sites of the metal's surface, thus helping to decrease the evolution of hydrogen. The adsorption of zwitterionic corrosion inhibitors (as a whole neutral) on the mild steel surface occurs through the displacement of adsorbed water molecules from the mild steel surface and sharing of the lone pair of electrons present in corrosion inhibitors, which decreases the anodic dissolution of metal.

4. Conclusions

The biogenic methionine residue and/or phosphonic acid in each repeating unit as a form of zwitterionic polymers were synthesized, characterized, and investigated in detail as corrosion inhibitors in 1 M HCl. The following conclusions were drawn from this study:

- The synthesized zwitterionic co-cyclopolymers showed very good performance for inhibiting/reducing the corrosion of mild steel in 1 M HCl.
- The inhibition efficiencies obtained from gravimetric weight loss, potentiodynamic polarization, and electrochemical impedance spectroscopy measurements are in good agreement.
- The zwitterionic corrosion inhibitors were found to be mixed-type inhibitors, but were mainly influenced by anodic sites.
- The corrosion inhibitors were adsorbed on the metal surface by chemisorption and physisorption processes, and obeyed Langmuir adsorption isotherms.
- Increasing the concentration of corrosion inhibitors increased the R'_p and decreased the CPE values.
- The AFM, SEM-EDX, and XPS analyses showed that the corrosion inhibitors protect the mild steel from corrosion attack.

Funding: The Deanship of Scientific Research (DSR), King Fahd University of Petroleum and Minerals (KFUPM), Saudi Arabia funded this research through Internal Project number IN131047.

Acknowledgments: The author gratefully acknowledges the Chemistry Department, KFUPM for providing excellent research facilities. The author is also thankful to Mumtaz A. Quraishi, Chair Professor, Center of Research Excellence in Corrosion, KFUPM, for valuable comments and suggestions on the presentation and quality of the manuscript.

Conflicts of Interest: The author declares no conflict of interest.

References

1. Mosa, J.; Rosero-Navarro, N.C.; Aparicio, M. Active corrosion inhibitor of mild steel by environmentally friendly Ce-doped organic-inorganic sol-gel coatings. *RSC Adv.* **2016**, *6*, 39577–39586. [[CrossRef](#)]

2. Fernandes, C.M.; Fagundes, T.S.F.; Santos, N.E.; Rocha, T.S.M.; Garrett, R.; Borges, R.M.; Muricy, G.; Valverde, A.L.; Ponzi, E.A. Ircinia strobilina crude extract as corrosion inhibitor for mild steel in acid medium. *Electrochim. Acta* **2019**, *312*, 137–148. [[CrossRef](#)]
3. Goyal, M.; Kumar, S.; Bahadur, I.; Verma, C.; Ebenso, E.E. Organic corrosion inhibitors for industrial cleaning of ferrous and non-ferrous metals in acidic solutions: A review. *J. Mol. Liq.* **2018**, *256*, 565–573. [[CrossRef](#)]
4. Mourya, P.; Banerjee, S.; Rastogi, R.B.; Singh, M.M. Inhibition of mild steel corrosion in hydrochloric acid and sulfuric acid media using thiosemicarbazone derivative. *Ind. Eng. Chem. Res.* **2013**, *52*, 12733–12747. [[CrossRef](#)]
5. James, A.O.; Oforka, N.; Olusegun, K.A. Inhibition of acid corrosion of mild steel by pyridoxal and pyridoxol hydrochlorides. *Int. J. Electrochem. Sci.* **2007**, *2*, 278–284.
6. Odoemelam, S.A.; Eddy, N.O. Effect of pyridoxal hydro-chloride-2,4-dinitrophenyl hydrazone on the corrosion of mild steel in hydrochloric acid. *Surf. Sci. Technol.* **2008**, *24*, 65–78.
7. Lgaz, H.; Bhat, K.S.; Salghi, R.; Jodeh, S.; Algarra, M.; Hammouti, B.; Ali, I.H.; Essamri, A. Insights into corrosion inhibition behavior of three chalcone derivatives for mild steel in hydrochloric acid solution. *J. Mol. Liq.* **2017**, *238*, 71–83. [[CrossRef](#)]
8. Pandey, A.; Singh, B.; Verma, C.; Ebenso, E.E. Synthesis, characterization and corrosion inhibition potential of two novel Schiff bases on mild steel in acidic medium. *RSC Adv.* **2017**, *7*, 47148–47163. [[CrossRef](#)]
9. TrabANELLI, G.; CaraaITI, V. *Corrosion Science and Technology*; Fontana, M.G., Staehle, R.W., Eds.; Plenum Press: New York, NY, USA, 1970; Volume 1, p. 147.
10. Kiani, M.A.; Mousavi, M.F.; Ghasemi, S.; Shamsipur, M.; Kazemi, S.H. Inhibitory effect of some amino acids on corrosion of Pb–Ca–Sn alloy in sulfuric acid solution. *Corros. Sci.* **2008**, *50*, 1035–1045. [[CrossRef](#)]
11. Rajeev, P.; Surendranathan, O.; Murthy, C.S.N. Corrosion mitigation of the oil well steels using organic inhibitors—A review. *J. Mater. Environ. Sci.* **2012**, *3*, 856–869.
12. Kumar, S.; Vashisht, H.; Olasunkanmi, L.O.; Bahadur, I.; Verma, H.; Goyal, M.; Singh, G.; Ebenso, E.E. Polyurethane based triblock copolymers as corrosion inhibitors for mild steel in 0.5 M H₂SO₄. *Ind. Eng. Chem. Res.* **2017**, *56*, 441–456. [[CrossRef](#)]
13. Baskar, R.; Gopiraman, M.; Kesavan, D.; Subramanian, K.; Gopalakrishnan, S. Utilization of photo-cross-linkable polymer for mild steel corrosion inhibition in 1.0 M HCl medium. *J. Mater. Eng. Perform.* **2015**, *24*, 2847–2856. [[CrossRef](#)]
14. Bacsikai, R.; Schroeder, A.H.; Young, D.C. Hydrocarbon-soluble alkyl aniline /formaldehyde oligomers as corrosion inhibitors. *J. Appl. Polym. Sci.* **1991**, *42*, 2435–2441. [[CrossRef](#)]
15. Kralji, M.; Mandi, Z.; Dui, L.J. Inhibition of steel corrosion by polyaniline coatings. *Corros. Sci.* **2003**, *45*, 181–198. [[CrossRef](#)]
16. Yan, R.; He, W.; Zhai, T.; Ma, H. Anticorrosion organic inorganic hybrid films constructed on iron substrates using self-assembled polyacrylic acid as a functional bottom layer. *Electrochim. Acta* **2019**, *295*, 942–955. [[CrossRef](#)]
17. Sheldon, R.A. Green and sustainable manufacture of chemicals from biomass: State of the art. *Green Chem.* **2014**, *16*, 950–963. [[CrossRef](#)]
18. El-Hafez, G.M.A.; Badawy, W.A. The use of cysteine, N-acetyl cysteine and methionine as environmentally friendly corrosion inhibitors for Cu–10Al–5Ni alloy in neutral chloride solutions. *Electrochim. Acta* **2013**, *108*, 860–866. [[CrossRef](#)]
19. Zhao, H.; Zhang, X.; Ji, L.; Hud, H.; Li, Q. Quantitative structure—Activity relationship model for amino acids as corrosion inhibitors based on the support vector machine and molecular design. *Corros. Sci.* **2014**, *83*, 261–271. [[CrossRef](#)]
20. Zhang, D.-Q.; Cai, Q.-R.; He, X.-M.; Gao, L.-X.; Kim, G.S. Corrosion inhibition and adsorption behavior of methionine on copper in HCl and synergistic effect of zinc ions. *Mater. Chem. Phys.* **2009**, *114*, 612–617. [[CrossRef](#)]
21. Zor, S.; Kandemirli, F.; Bingul, M. Inhibition effects of methionine and tyrosine on corrosion of iron in HCl solution: Electrochemical, FTIR, and Quantum-Chemical Study. *Prot. Met. Phys. Chem. Surf.* **2009**, *45*, 46–53. [[CrossRef](#)]
22. Shanmugasundaram, P.; Sumathi, T.; Chandramohan, G.; Ramesh-Bapu, G.N.K. Corrosion inhibition study of Is: 1062 grade A-low carbon steel in 1 M HCl by L–Methionine-weight loss, ICP-OES and SEM-EDX studies. *Int. J. Curr. Res.* **2013**, *5*, 2183–2189.

23. Oguzie, E.E.; Li, Y.; Wang, F.H. Corrosion inhibition and adsorption behavior of methionine on mild steel in sulfuric acid and synergistic effect of iodide ion. *J. Colloid Interface Sci.* **2007**, *310*, 90–98. [[CrossRef](#)] [[PubMed](#)]
24. Hammouti, B.; Aouniti, A.; Taleb, M.; Brighli, M.; Kertit, S. L-Methionine methyl ester hydrochloride as a corrosion inhibitor of iron in acid chloride solution. *Corrosion* **1995**, *51*, 411–416. [[CrossRef](#)]
25. Khaled, K.F. Corrosion control of copper in nitric acid solutions using some amino acids—A combined experimental and theoretical study. *Corros. Sci.* **2010**, *52*, 3225–3234. [[CrossRef](#)]
26. Verma, C.; Quraishi, M.; Kluza, K.; Makowska-Janusik, M.; Olasunkanmi, L.O.; Ebenso, E.E. Corrosion inhibition of mild steel in 1M HCl by D-glucose derivatives of dihydropyrido [2,3-d:6,5-d'] dipyrimidine-2, 4, 6, 8(1H,3H, 5H,7H)-tetraone. *Sci. Rep.* **2017**, *7*, 44432. [[CrossRef](#)] [[PubMed](#)]
27. Haque, J.; Srivastava, V.; Verma, C.; Lgaz, H.; Salghi, R.; Quraishi, M. N-Methyl-N,N,N-trioctylammonium chloride as a novel and green corrosion inhibitor for mild steel in an acid chloride medium: Electrochemical, DFT and MD studies. *New J. Chem.* **2017**, *41*, 13647–13662. [[CrossRef](#)]
28. Gupta, N.K.; Verma, C.; Salghi, R.; Lgaz, H.; Mukherjee, A.; Quraishi, M. New phosphonate based corrosion inhibitors for mild steel in hydrochloric acid useful for industrial pickling processes: Experimental and theoretical approach. *New J. Chem.* **2017**, *41*, 13114–13129. [[CrossRef](#)]
29. Hackerman, N.; Hurd, R.M. *Proceedings of the first International Congress of Metallic Corrosion*; Butterworths: London, UK, 1962.
30. Revie, W.; Uhlig, H.H. *Corrosion and Corrosion Control: An Introduction to Corrosion Science and Engineering*; Wiley-Inter Science: New York, NY, USA, 2008.
31. Butler, G.B. Cyclopolymerization. *J. Polym. Sci. Part A Polym. Chem.* **2000**, *38*, 3451–3461. [[CrossRef](#)]
32. Butler, G.B. *Cyclopolymerization and Cyclocopolymerization*; Marcel Dekker: New York, NY, USA, 1992.
33. Singh, P.K.; Singh, V.K.; Singh, M. Zwitterionic polyelectrolytes: A review. *E-Polymers* **2007**, *7*, 1–34. [[CrossRef](#)]
34. Jaeger, W.; Bohrisch, J.; Laschewsky, A. Synthetic polymers with quaternary nitrogen atoms- synthesis and structure of the most used type of cationic polyelectrolytes. *Prog. Polym. Sci.* **2010**, *35*, 511–577. [[CrossRef](#)]
35. Al-Muallem, H.A.; Mazumder, M.A.J.; Estaitie, M.K.; Ali, S.A. A novel cyclopolymer containing residues of essential amino acid methionine: Synthesis and application. *Iran. Polym. J.* **2015**, *24*, 541–547. [[CrossRef](#)]
36. Ali, S.A.; Goni, L.K.M.O.; Mazumder, M.A.J. Butler's cyclopolymerization protocol in the synthesis of diallylamine salts/sulfur dioxide alternate polymers containing amino acid residues. *J. Polym. Res.* **2017**, *24*, 184–195. [[CrossRef](#)]
37. Abu-Thabit, N.Y.; Kazi, I.W.; Al-Muallem, H.A.; Ali, S.A. Phosphonobetaine/sulfur dioxide copolymer by Butler's cyclopolymerization process. *Eur. Polym. J.* **2011**, *47*, 1113–1123. [[CrossRef](#)]
38. Kazi, I.W.; Rahman, F.; Ali, S.A. Synthesis of a polyphosphonate and its evaluation as an antiscalant in desalination Plant. *Polym. Eng. Sci.* **2014**, *54*, 166–174. [[CrossRef](#)]
39. Mazumder, M.A.J.; Al-Muallem, H.A.; Ali, S.A. The effects of N-pendants and electron-rich amidine motifs in 2(p-alkoxyphenyl)-2-imidazolines on mild steel corrosion in CO₂-saturated 0.5 M NaCl. *Corros. Sci.* **2015**, *90*, 54–68. [[CrossRef](#)]
40. Mazumder, M.A.J. Synthesis, characterization and electrochemical analysis of cysteine modified polymers for corrosion inhibition of mild steel in aqueous 1 M HCl. *RSC Adv.* **2019**, *9*, 4277–4294. [[CrossRef](#)]
41. Hegazy, M.A.; Badwai, A.M.; Abd El Rehim, S.S.; Kamel, W.M. Corrosion inhibition of carbon steel using novel N-(2-(2-mercaptoacetoxy) ethyl)-N,N-dimethyl dodecan-1-aminium bromide during acid pickling. *Corros. Sci.* **2013**, *69*, 110–122. [[CrossRef](#)]
42. Fragoza-Mar, L.; Olivares-Xometl, O.; Domínguez-Aguilar, M.A.; Flores, E.A.; Arellanes- Lozada, P.; Jimenez-Cruz, F. Corrosion inhibitor activity of 1,3-diketone malonates for mild steel in aqueous hydrochloric acid solution. *Corros. Sci.* **2012**, *61*, 171–184. [[CrossRef](#)]
43. Aljourani, J.; Raeissi, K.; Golozar, M.A. Benzimidazole and its derivatives as corrosion inhibitors for mild steel in 1M HCl solution. *Corros. Sci.* **2009**, *51*, 1836–1843. [[CrossRef](#)]
44. Vračar, L.M.; Drazic, D.M. Adsorption and corrosion inhibitive properties of some organic molecules on iron electrode in sulfuric acid. *Corros. Sci.* **2002**, *44*, 1669–1680. [[CrossRef](#)]
45. Ansari, K.R.; Quraishi, M.A.; Singh, A. Isatin derivatives as a non-toxic corrosion inhibitor for mild steel in 20% H₂SO₄. *Corros. Sci.* **2015**, *95*, 62–70. [[CrossRef](#)]
46. Wang, X.; Yang, H.; Wang, F. An investigation of benzimidazole derivative as corrosion inhibitor for mild steel in different concentration HCl solutions. *Corros. Sci.* **2011**, *53*, 113–121. [[CrossRef](#)]

47. Okafor, P.C.; Liu, X.; Zheng, Y.G. Corrosion inhibition of mild steel by ethyl amino imidazoline derivative in CO₂-saturated solution. *Corros. Sci.* **2009**, *51*, 761–768. [[CrossRef](#)]
48. Khamis, A.; Saleh, M.M.; Awad, M.I.; El-Anadouli, B.E. Enhancing the inhibition action of cationic surfactant with sodium halides for mild steel in 0.5 M H₂SO₄. *Corros. Sci.* **2013**, *74*, 83–91. [[CrossRef](#)]
49. Tourabi, M.; Nohair, K.; Traisnel, M.; Jama, C.; Bentiss, F. Electrochemical and XPS studies of the corrosion inhibition of carbon steel in hydrochloric acid pickling solutions by 3,5-bis(2-thienylmethyl)-4-amino-1,2,4-triazole. *Corros. Sci.* **2013**, *75*, 123–133. [[CrossRef](#)]
50. Morad, M.S.; El-Dean, A.M.K. 2,2'-Dithiobis(3-cyano-4,6-dimethylpyridine): A new class of acid corrosion inhibitors for mild steel. *Corros. Sci.* **2006**, *48*, 3398–3412. [[CrossRef](#)]
51. Mu, G.N.; Li, X.H.; Qu, Q.; Zhou, J. Molybdate and tungstate as corrosion inhibitors for cold rolling steel in hydrochloric acid solution. *Corros. Sci.* **2006**, *48*, 445–459. [[CrossRef](#)]
52. Zhang, F.; Tang, Y.; Cao, Z.; Jing, W.; Wu, Z.; Chen, Y. Performance and theoretical study on corrosion inhibition of 2-(4-pyridyl)-benzimidazole for mild steel in hydrochloric acid. *Corros. Sci.* **2012**, *61*, 1–9. [[CrossRef](#)]
53. Motamedi, M.; Tehrani-Bagha, A.R.; Mahdavian, M. Effect of aging time on corrosion inhibition of cationic surfactant on mild steel in sulfamic acid cleaning solution. *Corros. Sci.* **2013**, *70*, 46–54. [[CrossRef](#)]
54. Qu, Q.; Jiang, S.A.; Bai, W.; Li, L. Effect of ethylenediamine tetraacetic acid disodium on the corrosion of cold rolled steel in the presence of benzotriazole in hydrochloric acid. *Electrochim. Acta* **2007**, *52*, 6811–6820. [[CrossRef](#)]
55. Negma, N.A.; Kandile, N.G.; Badr, E.A.; Mohammed, M.A. Gravimetric and electrochemical evaluation of environmentally friendly nonionic corrosion inhibitors for carbon steel in 1 M HCl. *Corros. Sci.* **2012**, *65*, 94–103. [[CrossRef](#)]
56. Sahayaraja, A.S.; Rajendran, S. Inhibition of corrosion of carbon steel in well water by arginine- Zn²⁺ system. *J. Electrochem. Sci. Eng.* **2012**, *2*, 91–104.
57. Ptasinska, S.; Stypczyńska, A.; Nixon, T.; Mason, N.J.; Klyachko, D.V.; Sanche, L. X-ray induced damage in DNA monitored by X-ray photoelectron spectroscopy. *J. Chem. Phys.* **2008**, *129*, 08B604. [[CrossRef](#)] [[PubMed](#)]
58. Zarrok, H.; Zarrouk, A.; Hammouti, B.; Salghi, R.; Jama, C.; Bentiss, F. Corrosion control of carbon steel in phosphoric acid by purpald—Weight loss, electrochemical and XPS studies. *Corros. Sci.* **2012**, *64*, 243–252. [[CrossRef](#)]
59. Behpour, M.; Ghoreishi, S.M.; Salavati-Niasari, M.; Ebrahimi, B. Evaluating two new synthesized S–N Schiff bases on the corrosion of copper in 15% hydrochloric acid. *Mater. Chem. Phys.* **2008**, *107*, 153–157. [[CrossRef](#)]
60. Bentiss, F.; Mernari, B.; Traisnel, M.; Vezin, H.; Lagrenee, M. On the relationship between corrosion inhibiting effect and molecular structure of 2,5-bis(n-pyridyl)-1,3,4-thiadiazole derivatives in acidic media: Ac impedance and DFT studies. *Corros. Sci.* **2011**, *53*, 487–495. [[CrossRef](#)]
61. Ansari, K.R.; Quraishi, M.A. Bis-Schiff bases of isatin as new and environmentally benign corrosion inhibitor for mild steel. *J. Ind. Eng. Chem.* **2014**, *20*, 2819–2829. [[CrossRef](#)]
62. Ahamad, I.; Khan, S.; Ansari, K.R.; Quraishi, M.A. Primaquine: A pharmaceutically active compound as corrosion inhibitor for mild steel in hydrochloric acid solution. *J. Chem. Pharm. Res.* **2011**, *3*, 703–717.
63. Ituen, E.; Akaranta, O.; James, A. Evaluation of performance of corrosion inhibitors using adsorption isotherm models: An overview. *Chem. Sci. Int. J.* **2016**, *18*, 1–34. [[CrossRef](#)]
64. Saxena, A.; Prasad, D.; Haldhar, R.; Singh, G.; Kumar, A. Use of sida cordifolia extract as green corrosion inhibitor for mild steel in 0.5 M H₂SO₄. *J. Environ. Chem. Eng.* **2018**, *6*, 694–700. [[CrossRef](#)]

